Mon. Not. R. Astron. Soc. **306**, 779–798 (1999)

Statistical characteristics of formation and evolution of structure in the Universe

M. Demiański[1,2] and A. G. Doroshkevich[3,4]

[1]*Institute of Theoretical Physics, University of Warsaw, 00-681 Warsaw, Poland*
[2]*Department of Astronomy, Williams College, Williamstown, MA 01267, USA*
[3]*Theoretical Astrophysics Center, Juliane Maries Vej 30, DK-2100 Copenhagen Ø, Denmark*
[4]*Keldysh Institute of Applied Mathematics, Russian Academy of Sciences, 125047 Moscow, Russia*

Accepted 1999 February 10. Received 1999 February 1; in original form 1998 October 12

ABSTRACT

An approximate statistical description of the formation and evolution of structure of the Universe based on the Zel'dovich theory of gravitational instability is proposed. It is found that the evolution of dark matter (DM) structure shows features of self-similarity and the main structure characteristics can be expressed through the parameters of the initial power spectrum and cosmological model. For the CDM-like power spectrum and suitable parameters of the cosmological model the effective matter compression reaches the observed scales $R_{\rm wall} \sim 20$–$25h^{-1}$ Mpc with the typical mean separation of wall-like elements $D_{\rm SLSS} \sim 50$–$70h^{-1}$ Mpc. This description can be directly applied to the deep pencil beam galactic surveys and absorption spectra of quasars. For larger 3D catalogues and simulations it can be applied to results obtained with the core-sampling analysis.

It is shown that the interaction of large- and small-scale perturbations modulates the creation rate of early Zel'dovich pancakes and generates bias on the SLSS scale. For suitable parameters of the cosmological model and reheating process this bias can essentially improve the characteristics of simulated structure of the Universe.

The models with $0.3 \leq \Omega_{\rm m} \leq 0.5$ give the best description of the observed structure parameters. The influence of low-mass 'warm' dark matter particles, such as a massive neutrino, will extend the acceptable range of $\Omega_{\rm m}$ and h.

Key words: galaxies: clusters: general – cosmology: theory – large-scale structure of Universe.

1 INTRODUCTION

Over the past decade the large maps of the spatial galaxy distribution have been prepared and the unexpectedly complicated character of this distribution was established. The structure predicted by the Zel'dovich theory of gravitational instability (Zel'dovich 1970, 1978) was found already in the first wedge diagrams (Gregory & Thompson 1978) and now the large-scale structure (LSS) is seen in many observational catalogues, such as the CfA (de Lapparent, Geller & Huchra 1988; Ramella, Geller & Huchra 1992), the SRSS (da Costa et al. 1988) and in the Las Campanas Redshift Survey (Shectman et al. 1996, hereafter LCRS). The observed high concentration of galaxies within the wall-like structure elements such as the Great Attractor (Dressler et al. 1987), and the Great Wall (de Lapparent, Geller & Huchra 1988) and the existence of extended under dense regions similar to the Great Void (Kirshner et al. 1983) put in the forefront the investigation of the super large-scale structure (SLSS). Now the SLSS is also found in many deep pencil-beam redshift surveys (Broadhurst et al. 1990; Willmer et al. 1994; Buryak, Doroshkevich & Fong 1994 ; Bellanger & de Lapparent 1995; Cohen et al. 1996) as a rich galaxy clumps with the typical separations in the range of $(60$–$120)h^{-1}$ Mpc. Here $h = H_0/100\,{\rm km\,s^{-1}\,Mpc^{-1}}$ is the dimensionless Hubble constant.

Further progress in the statistical description of the LSS and SLSS has been reached with the core-sampling method (Buryak, Doroshkevich & Fong 1994) and the Minimal Spanning Tree technique (Barrow, Bhavsar & Sonoda 1985). Recent analysis of the LCRS performed by Doroshkevich et al. (1996, 1997b, hereafter LCRS1 and LCRS2 respectively, 1998b) revealed some statistical parameters of the wall-like SLSS component such as their typical separation, $D_{\rm SLSS} \approx 50$–$60h^{-1}$ Mpc, and the fraction of galaxies accumulated by the SLSS, which can reach ~50 per cent. The same analysis indicates that formation of richer walls can be roughly described as an asymmetric 2D collapse of regions with a typical size $R_{\rm wall} \sim 20$–$25h^{-1}$ Mpc that is about half of their typical separation. The analysis of Durham/UKST redshift survey confirms these results (Doroshkevich et al. 1999b). Earlier similar scales, in the range of 50–$100h^{-1}$ Mpc, were found only for spatial distribution of clusters of galaxies (see, e.g., Bahcall

1988; Einasto et al. 1994) and for a few superclusters of galaxies (see, e.g., Oort 1983a,b).

Evolution of structure was discussed and simulated many times (see, e.g., Sahni, Sathyaprakash & Shandarin 1994; Doroshkevich et al. 1997a, hereafter DFGMM; for references, Sahni & Coles 1995). However, SLSS in the dark matter (DM) distribution similar to that seen in the LCRS was found only recently in a few simulations with the CDM-like power spectrum and $\Omega_{\rm m}h = 0.2$–0.3, (Cole et al. 1997; Doroshkevich et al. 1999a, hereafter DMRT). Hence, for suitable cosmological models the evolution of small initial perturbations results in the SLSS formation.

In this paper we present an approximate statistical description of the process of DM structure formation based on the non-linear Zel'dovich theory. The potential of this approach is limited as the successive consideration of mutual interactions of the small- and large-scale perturbations becomes more and more cumbersome. In spite of this it allows us to obtain some interesting results. Thus, it is shown that formation of both LSS and SLSS is a joint process possessing some features of self-similarity. The main observed characteristics of LSS and SLSS are expressed through the structure functions of power spectrum and through the typical scales, set by the power spectrum, the time-scale, set by the amplitude of perturbation, and the main parameters of cosmological model. One of the most interesting such characteristics is the dynamical scale of the non-linearity defined as the scale of essential DM concentration within high density walls. We show that for the CDM transfer function (Bardeen et al. 1986, hereafter BBKS) and Harrison–Zel'dovich primordial power spectrum and for cosmological models with lower matter density this scale of non-linearity reaches 20–$30h^{-1}\,$Mpc, which is comparable with typical scales of the observed SLSS elements.

Simulations (DMRT) show that even in cosmological models with a low matter density the simulated velocity dispersion within the SLSS elements reaches 400–$700\,{\rm km\,s^{-1}}$ *along each principal axis*; this exceeds the observed value by a factor of ~ 1.5–2. Such a large and isotropic velocity dispersion is caused by the disruption of the walls into high density clouds. For smaller matter density of the Universe this dispersion decreases but together with the fraction of matter accumulated by the walls. This means that other factors as, for example, the large-scale bias in the spatial galaxy distribution relative to the more homogeneous distribution of DM and baryons could be essential for the successful reproduction of the observed SLSS. Such large-scale bias caused by the interaction of small- and large-scale perturbations was discussed by Dekel & Silk (1986), and Dekel & Rees (1987), and estimated by Demiański & Doroshkevich (1999, hereafter Paper I).

The interaction of small- and large-scale perturbations is important during all evolutionary stages. Thus, even during early evolutionary periods the large-scale perturbations modulate the rate of pancake formation. This modulation is seen as an acceleration of the pancake formation within deeper potential wells which later are transformed into the wall-like SLSS elements (Buryak, Demiański & Doroshkevich 1992; Demiański & Doroshkevich 1997; Paper I). Suppression of pancake formation near the peaks of gravitational potential noted by Sahni, Sathyaprakash & Shandarin (1994) is another manifestation of such interactions. During all evolutionary stages these interactions result in the successive merging of individual pancakes. The acceleration of pancake disruption, caused by compression of matter within walls, can also be attributed to this interaction. Now it is observed as a high-velocity dispersion in simulated SLSS and as differences between the expected and measured mass functions. It was found to be essential even for pancakes formed at high redshifts (Miralda-Escude et al. 1996). The possible correlation of galaxy morphology with large-scale perturbations was discussed by Evrard, Silk & Szalay (1990). All these manifestations of small- and large-scale interaction are important for the correct comparison and interpretation of simulated and observed matter distribution.

Now the modulation of spatial distribution of pancakes formed at high redshifts $z \geq 4$ can be seen as the large-scale bias in the galaxy and DM spatial distribution. This bias can be generated by the combined action of large-scale perturbations and reheating of baryonic component of the Universe (see, e.g., Dekel & Silk 1986; Dekel & Rees 1987). The reheating was discussed many times during the last thirty years in various aspects (see, e.g., Sunyaev & Zel'dovich 1972; White & Rees 1978; Shapiro, Giroux & Babul 1994). Effects of reheating on the process of galaxy formation were discussed as well (see, e.g., Babul & White 1991; Efstathiou 1992; Quinn, Katz & Efstathiou 1996). It is also known that under reasonable assumptions about the possible energy sources reheating can occur for relatively small range of redshifts $z \approx 5$–10 (see, e.g., Tegmark et al. 1997; Baltz, Gnedin & Silk 1998). If essential concentration of baryons in high-density clouds is reached at the same redshifts, the reheating can help to generate bias (Demiański & Doroshkevich 1997; Paper I). In this case further formation of high-density baryonic clouds will be significantly depressed, owing to reheating, within extended regions observed today as under dense regions between richer walls. Our estimates show that this spatial modulation of the luminous matter distribution may be essential for the interpretation of observations.

Numerical simulations are now the best way to reproduce and to study the joint action of all the pertinent factors together and to obtain more representative description of the process of structure formation. Essential progress achieved recently both in the simulations and study of DM and 'galaxy' distributions (Governato et al. 1998; Jenkins et al. 1998; Doroshkevich et al. 1998a; DMRT; Cole et al. 1998) allows us to follow the structure evolution in a wide range of redshifts and to reveal differences between DM and galaxy distribution. Comparison of these results with observations and an approximate theoretical description stimulates further progress in our understanding of evolution of the Universe.

This paper is organized as follows. In Section 2 main notations are introduced. In Sections 3 and 4 the distribution functions of DM pancakes are derived and the interaction of small- and large-scale perturbations is described that allows us to obtain in Sections 5 and 6 the statistical characteristics of DM structure. In Section 7 the large-scale bias is discussed and in Section 8 the dynamical characteristics of walls are found. In Section 9 the theoretical estimates are compared with the available observational and simulated data. We conclude with Section 10 where a short discussion of the main results is presented. Some technical details are given in Appendixes A to D.

2 STATISTICAL PARAMETERS OF PERTURBATIONS: VARIANCES AND TYPICAL SCALES

The simplest characteristics of perturbations are the variances of density and velocity perturbations. For a more detailed statistical description of the structure evolution it is necessary to use also the

structure functions. They were introduced in Paper I and are briefly described in this section and Appendix A. Here we consider only the SCDM-like power spectrum but the same approach can be applied for other spectra as well.

Our analysis is based on the Zel'dovich theory which links the Eulerian, r_i, and the Lagrangian, q_i, coordinates of fluid elements (particles) by the expression

$$r_i = (1+z)^{-1}[q_i - B(z)S_i(\boldsymbol{q})], \tag{2.1}$$

where z denotes the redshift, $B(z)$ describes growth of perturbations in the linear theory, and the potential vector $S_i(\boldsymbol{q}) = \partial\phi/\partial q_i$ characterizes the spatial distribution of perturbations. The Lagrangian coordinates of a particle, q_i, are its unperturbed comoving coordinates.

For the flat universe with $\Omega_\mathrm{m} + \Omega_\Lambda = 1$, $\Omega_\mathrm{m} \geq 0.1$, the function $B(z)$ can be approximated with a precision better than 10 per cent by the expression (Paper I)

$$B^{-3}(z) \approx \frac{1 - \Omega_\mathrm{m} + 2.2\Omega_\mathrm{m}(1+z)^3}{1 + 1.2\Omega_\mathrm{m}}, \tag{2.2}$$

and for an open universe with $0.1 \leq \Omega_\mathrm{m} \leq 1$, $\Omega_\Lambda = 0$ as

$$B^{-1}(z) \approx 1 + \frac{2.5\Omega_\mathrm{m}}{1 + 1.5\Omega_\mathrm{m}} z \tag{2.3}$$

(Zel'dovich & Novikov 1983). For $\Omega_\mathrm{m} = 1, \Omega_\Lambda = 0$ both expressions give $B^{-1}(z) = 1 + z$.

The main characteristics of the perturbations are the variances of density σ_ρ^2, displacement σ_s^2, and components of the deformation tensor σ_D^2

$$\sigma_s^2 = \frac{1}{2\pi^2}\int_0^\infty p(k)\mathrm{d}k, \quad \sigma_\rho^2 = 5\sigma_D^2 = \frac{1}{2\pi^2}\int_0^\infty p(k)k^2\mathrm{d}k, \tag{2.4}$$

where $p(k)$ is the power spectrum, and k is the comoving wave number.

The power spectrum determines also two amplitude independent typical scales, which allow us to describe the process of structure formation and can be, possibly, estimated from the observed galaxy distribution. For the Harrison–Zel'dovich primordial power spectrum these scales, l_0 and l_c, are defined as

$$l_0^{-2} = \int_0^\infty kT^2(k/k_0)\mathrm{d}k, \quad l_\mathrm{c}^2 = \frac{5}{3}\frac{\sigma_s^2}{\sigma_\rho^2}, \tag{2.5}$$

where $T^2(x)$ is the transfer function and $k_0 = \Omega_\mathrm{m}h^2\,\mathrm{Mpc}^{-1}$. For the CDM transfer function (BBKS) the scale l_0 and the typical masses of DM and baryonic components associated with the scale l_0 are

$$l_0 \approx 6.6(\Omega_\mathrm{m}h)^{-1}\sqrt{\frac{0.023}{m_{-2}}}h^{-1}\,\mathrm{Mpc}, \tag{2.6}$$

$$M_0 = \frac{\pi}{6}\langle\rho\rangle l_0^3 \approx \frac{2.5\times10^{13}\mathrm{M}_\odot}{\Omega_\mathrm{m}^2h^4}, \quad M_\mathrm{b}^{(0)} = \frac{\Omega_\mathrm{b}}{\Omega_\mathrm{m}}M_0.$$

$$m_{-2} = \int_0^\infty xT^2(x)\mathrm{d}x$$

For the SCDM power spectrum the σ_ρ^2 is divergent (logarithmically) at large k and the standard CDM transfer function should be truncated by introduction of an appropriate mass of DM particle, M_DM. This restriction allows, however, a significant interval for a possible mass of DM particles – up to 10^{16}–10^{20} eV. In this paper we will use the ratio l_c/l_0 as a measure of the mass of DM particles. For $0.5\,\mathrm{keV} \leq M_\mathrm{DM} \leq 10^{17}\,\mathrm{keV}$ we have $0.2 \geq l_\mathrm{c}/l_0 \geq 0.01$ and for $M_\mathrm{DM} \geq 5\,\mathrm{keV}$ the following approximate expression can be used

$$l_\mathrm{c}/l_0 \approx \frac{0.061}{\sqrt{\ln M_\mathrm{DM}}}, \tag{2.7}$$

$$M_\mathrm{c} = \left(\frac{l_\mathrm{c}}{l_0}\right)^3 M_0 \approx \frac{0.6\times10^{10}\mathrm{M}_\odot}{(\ln M_\mathrm{DM})^{3/2}\Omega_\mathrm{m}^2h^4},$$

where M_DM is the mass of DM particle in keV. It turns out that the final results only weakly depend on the mass of DM particles. For the Harrison–Zel'dovich primordial power spectrum the dependence of the moments and typical scales on the mass of DM particles was discussed in Paper I. More cumbersome correlation and structure functions of perturbations were also discussed in Paper I and, partly, are presented in the Appendix A.

The amplitude of power spectrum can be taken from the measured anisotropy of the relic radiation (Stompor, Gorski & Bandy 1995; Bunn & White 1997; Gorski et al. 1998). It can be fitted by

$$\sigma_s \approx 31.2\sqrt{\frac{m_{-2}}{0.023}}\left(\frac{T_\mathrm{Q}}{20\,\mu\mathrm{K}}\right)a(\Omega_\mathrm{m},\Omega_\Lambda)\ \mathrm{Mpc},$$

$$a(\Omega_\mathrm{m}, \Omega_\Lambda = 1-\Omega_\mathrm{m}) = \Omega_\mathrm{m}^{0.215-0.05\ln\Omega_\mathrm{m}}, \tag{2.8}$$

$$a(\Omega_\mathrm{m}, \Omega_\Lambda = 0) = \Omega_\mathrm{m}^{0.65-0.19\ln\Omega_\mathrm{m}}.$$

where T_Q is the amplitude of quadrupole component of anisotropy of the relic radiation. The time-scale of the structure evolution is defined by the function

$$\tau(z) = \tau_0 B(z),$$

$$\tau_0 = \frac{\sigma_s}{\sqrt{3}l_0} \approx 2.73h^2\Omega_\mathrm{m}\left(\frac{m_{-2}}{0.023}\frac{T_\mathrm{Q}}{20\,\mu\mathrm{K}}\right)a(\Omega_\mathrm{m},\Omega_\Lambda),$$

$$\tau_0 \approx 2.73h^2\Omega_\mathrm{m}^{1.21}\left(\frac{m_{-2}}{0.023}\frac{T_\mathrm{Q}}{20\,\mu\mathrm{K}}\right), \quad \Omega_\Lambda = 1-\Omega_\mathrm{m}, \tag{2.9}$$

$$\tau_0 \approx 2.73h^2\Omega_\mathrm{m}^{1.65-0.19\ln\Omega_\mathrm{m}}\left(\frac{m_{-2}}{0.023}\frac{T_Q}{20\,\mu\mathrm{K}}\right), \quad \Omega_\Lambda = 0, \Omega_\mathrm{m} \leq 1.$$

Further on, as a rule, the dimensionless variables will be used. We will use l_0 as the unit of length, and $\langle\rho\rangle l_0$ as the unit of surface density. This means also that such dimensionless characteristics of a pancake as the size of collapsed slab and resulting surface density of a pancake are identical. Below we will use both terms as well as the term 'mass', m, to characterize the surface density reached during formation of a pancake. The gravitational potential and displacement are measured in units of $\sigma_s l_0/\sqrt{3}$ and $\sigma_s/\sqrt{3}$, respectively.

3 STATISTICAL CHARACTERISTICS OF PANCAKES

In this section the mass function of Zel'dovich pancakes and its time evolution is given. This can be done using the main equation of Zel'dovich theory (2.1). The mass of compressed matter is measured by the Lagrangian size of compressed slab, q, or by the surface density of pancake, $\langle\rho\rangle q$. As it was noted above, both measures are identical in dimensionless notation. So, we will use

both terms 'size', q, and 'mass', m, of a pancake to characterize its surface density.

Here we do not consider the transversal characteristics of structure elements and cannot discriminate, for example, the central part of a poorer pancake and periphery of richer pancake, if they have the same surface density or mass, m. In this sense our approach gives characteristics similar to that obtained with the core-sampling analysis, pencil-beam observations or the distribution of absorption lines in spectra of QSOs.

3.1 The pancake formation

According to the relation (2.1) when two particles with different Lagrangian coordinates $\boldsymbol{q_1}$ and $\boldsymbol{q_2}$ meet at the same Eulerian point $\boldsymbol{r}$ a pancake with the surface mass density $\langle\rho\rangle|\boldsymbol{q}_1-\boldsymbol{q}_2|$ forms. Here we assume that *all* particles situated between these two boundary particles are also incorporated into the same pancake. This assumption is also made in the adhesion approach (see, e.g., Shandarin & Zel'dovich 1989). Formally, this condition can be written as

$$\boldsymbol{q}_{12}=\boldsymbol{q}_1-\boldsymbol{q}_2=\tau\cdot[\boldsymbol{S}(\boldsymbol{q}_1)-\boldsymbol{S}(\boldsymbol{q}_2)]. \tag{3.1}$$

This means that the pancake formation process can be characterized by the scalar random function

$$Q(q_{12})=\frac{\boldsymbol{q}_{12}}{q_{12}}\cdot[\boldsymbol{S}(\boldsymbol{q}_1)-\boldsymbol{S}(\boldsymbol{q}_2)] \tag{3.2a}$$

under the condition

$$\boldsymbol{q}_{12}\times[\boldsymbol{S}(\boldsymbol{q}_1)-\boldsymbol{S}(\boldsymbol{q}_2)]=0.$$

In a coordinate system with the first axis oriented along the vector $\boldsymbol{q}_{12}$ the condition (3.1) can be rewritten more explicitly as

$$Q(q_{12})=\Delta S_1=q_{12}/\tau,\Delta S_2(q_{12})=\Delta S_3(q_{12})=0,$$

$$\Delta S_i=S_i(\boldsymbol{q}_1)-S_i(\boldsymbol{q}_2), \tag{3.2b}$$

and formation of a pancake is described by the 1D matter flow between points $q_1=\boldsymbol{q}_1\cdot\boldsymbol{q}_{12}/q_{12}$ and $q_2=\boldsymbol{q}_2\cdot\boldsymbol{q}_{12}/q_{12}$.

As is shown in Appendix B, under the assumption of Gaussian distribution of perturbations and neglecting the (weak) correlations between matter motion in orthogonal directions, the probability of a pancake formation, for a given q prior to the 'time' τ or for a given τ with a size larger then q, is identical to the probability to have $\Delta S_1\geq q/\tau$ $[Q(q_{12})/q_{12}\geq 1/\tau]$, so

$$W_{\rm cr}(>q,\tau)=1-\frac{1}{8}\left[1+{\rm erf}\left(\frac{\mu(q)}{\sqrt{2}\tau}\right)\right]^3,$$

$$\mu(q)=\frac{q}{\sqrt{2[1-G_{12}(q)]}}. \tag{3.3}$$

where (see Appendices A and B)

$$\mu(q)\approx\sqrt{q_0/3},\quad q<q_0,$$

$$\mu(q)\approx\sqrt{q}/2,\quad q_0\ll q<1,\quad \mu(q)\approx q/\sqrt{2},\quad q\gg 1, \tag{3.4}$$

$$q_0\approx 6l_{\rm c}^2/l_0^2\approx\frac{0.022}{\ln M_{\rm DM}},\quad M_q=q_0^3M_0\approx\frac{3\times10^8\,{\rm M}_\odot}{(\ln M_{\rm DM})^3\Omega_{\rm m}^2h^4}.$$

As is seen from (3.1), and (3.3) the pancake characteristics at the moment τ are expressed through the function $\mu(q)$ related to the initial power spectrum. This is an essential feature of the Zel'dovich theory allowing one to obtain approximate analytical description of pancake properties.

Equation (3.3) demonstrates that $\sim\frac{7}{8}$ of matter with $Q(q_{12})\geq 0$ is compressed at least in one direction and for $\sim\frac{1}{8}$ of matter 3D expansion takes place what reflects the symmetry of initial distribution of the displacements, ΔS_i. At first glance it seems that this conclusion is in contradiction with known results of Zel'dovich theory. Actually, the fraction of mass, $f_{\rm DM}$, accumulated by pancakes can be estimated using the PDF for the largest principal value of deformation tensor, ${\rm d}W(\lambda_1)$, (Zel'dovich 1970; Doroshkevich 1970; Doroshkevich & Shandarin 1979; Shandarin & Zel'dovich 1989; Paper I). This PDF can be approximated (with a precision $\sim$10 per cent) by the Gaussian function with $\langle\lambda_1\rangle=3\sigma_D/\sqrt{2\pi}$, $\sigma_\lambda^2=(13/6-4.5/\pi)\sigma_D^2$. As in the Zel'dovich theory pancake formation is described by the relation $B(z)\lambda_1=1$ [which follows directly from (2.1)], so for the fraction of compressed matter with $\lambda_1\geq 1/B$ we have

$$f_{\rm DM}\approx\frac{1}{2}{\rm erfc}\left[\frac{\sigma_D}{\sqrt{2}\sigma_\lambda}\left(\frac{l_{\rm c}}{l_0\tau}-\frac{3}{\sqrt{2\pi}}\right)\right] \tag{3.5}$$

and for $\tau\gg l_{\rm c}/l_0$, $f_{\rm DM}\to 1$ (in the Zel'dovich theory $0.92\leq f_{\rm DM}\leq 1$). This shows that already during the early period of non-linear evolution, at $\tau\approx l_{\rm c}/l_0\ll 1$, large fraction of matter $f_{\rm DM}\geq 0.9$ is compressed into low-mass pancakes. However, for the CDM-like power spectrum the description of matter compression through the deformation tensor is appropriate only at small scales $q\leq q_0$ whereas for $q\gg q_0$, the correlations between matter flow in orthogonal directions rapidly decrease what can be seen directly from the expressions for the structure functions given in Appendix A.

At larger scales we have to use the more cumbersome description discussed above and the estimate (3.3) shows that at such scales the efficiency of matter integration into structure elements is only ~ 0.875 (more accurate estimates taking into account the correlation of displacements lowers this value to 0.79). This limit is reached already at small τ, for $q\ll 1$, that means strong matter concentration within small structure elements. Further evolution does not change this limit and only redistributes – owing to sequential merging – the compressed matter to more and more massive structure elements. Thus, the approximate estimates show that $\sim$21 per cent of matter is subjected to 3D compression, $\sim$21 per cent to 3D expansion, $\sim$29 per cent of matter is subjected to 2D compression and can be accumulated by filaments and $\sim$29 per cent is subjected to 1D compression and remains in pancakes. The difference between estimates (3.3) and (3.5) shows that $\sim$15–20 per cent of matter incorporated in small clouds, with $M\leq M_q$, is not accumulated by larger pancakes, with $M\geq M_q$, and remains distributed between those pancakes. These estimates can be changed because the Zel'dovich approximation becomes invalid when strong matter compression is reached during pancake formation.

3.2 The characteristics of pancake formation

The probability distribution function (PDF) for pancakes formed at the moment τ can be found from (3.3) as

$$N_{\rm cr}(q,\tau)=-\frac{8}{7}\frac{{\rm d}W_{\rm cr}}{{\rm d}q}=\frac{6}{7\sqrt{2\pi}\tau}\frac{{\rm d}\mu}{{\rm d}q}\Phi\left(\frac{\mu}{\sqrt{2}\tau}\right),\quad 0<q<\infty, \tag{3.6}$$

$$\Phi(x)={\rm e}^{-x^2}[1+{\rm erf}(x)]^2.$$

Simple analysis based on relations (3.3), (3.6) shows that the maximum of the PDF (3.6) is reached at $q \approx 1.5q_0 \ll 1$.

The mean mass (surface density) of formed pancakes is described by the expression

$$\langle m(\tau)\rangle = \int_0^\infty qN_{\rm cr}{\rm d}q = \frac{8}{7}\int_0^\infty W_{\rm cr}{\rm d}q, \tag{3.7}$$

$$\langle m(\tau)\rangle \approx 4\tau^2, \quad \tau \ll 1, \quad \langle m(\tau)\rangle \approx \tau, \quad \tau \geq 1,$$

and the mass distribution is characterized by the function

$$N_{\rm cr}^{(m)} = \frac{6}{7\sqrt{2\pi}\tau}\frac{q}{\langle m\rangle}\frac{{\rm d}\mu}{{\rm d}q}\Phi\left(\frac{\mu}{\sqrt{2}\tau}\right). \tag{3.8}$$

The rate of formation of pancakes with mass q is

$$N_\tau = \frac{8}{7}\frac{{\rm d}W_{\rm cr}}{{\rm d}\tau}(q,\tau) = \frac{6}{7\sqrt{2\pi}}\frac{\mu}{\tau^2}\Phi\left(\frac{\mu}{\sqrt{2}\tau}\right), \tag{3.9}$$

and the maximal rate is reached for $\mu(q) \approx \tau$.

These relations take into account the growth of pancake size owing to accretion of matter and form a reliable basis for further theoretical considerations of various characteristics of structure elements. However they cannot be applied directly to the observed and simulated matter distribution as they do not consider the possibility of merging of pancakes. In the process of merging, earlier formed pancakes are accumulated by larger ones. A more refined technique taking into account the pancake interaction should be used in order to describe the evolution of *structure elements* that are the pancakes that survived the merging process. The same problem appears in the Press–Schechter theory and it can be solved by introduction of the survival probability (Peacock & Heavens 1990; Bond et al. 1991). This problem will be discussed below.

3.3 Spatial characteristics of pancake distribution

Using the standard technique (see, e.g., BBKS) we can also find the mean cumulative comoving linear number density of pancakes, $n(>q)$, which characterizes the pancake distribution along a random straight line

$$n(>q){\rm d}r = \frac{3}{4\sqrt{2\pi}}\frac{\mu(q)}{q}\langle\nabla Q\cdot{\rm d}\boldsymbol{r}\rangle\Phi\left(\frac{\mu}{\sqrt{2}\tau}\right).$$

When $l_{\rm c} \ll l_0$ it is described by the following (approximate) expression:

$$n(>q) \approx \frac{3\langle\mu_r\rangle}{4\pi\sqrt{q_0}}[\sqrt{6}+\ln(\sqrt{3}+\sqrt{2})]\frac{\mu(q)}{q}\Phi\left(\frac{\mu}{\sqrt{2}\tau}\right),$$

$$l_{\rm c}n(>q) \approx \frac{1.35}{\sqrt{6}\pi}\frac{\mu(q)}{q}\Phi\left(\frac{\mu}{\sqrt{2}\tau}\right), \tag{3.10}$$

where $\langle\mu_r\rangle = 0.5$ describes the random orientation of a pancake and the chosen straight line (see also Appendix B).

To characterize the 3D distribution of higher peaks of the function $Q(q)$ and the percolation process, in the course of which separate pancakes are integrated into the joint structure, the standard technique using the Euler characteristics can be applied. It is described in detail by BBKS, Gott et al. (1989), Coles, Davies & Pearson (1996) and Seto et al. (1997).

In our case the anisotropy of the pancake compression manifests itself as an anisotropy of correlation functions of displacements and their derivatives what results in the appearance of different Euler characteristics, $n_{31}(q,\tau)$, $n_{32}(q,\tau)$, $n_{33}(q,\tau)$:

$$n_{31} = \frac{3}{32\pi^2}\frac{\langle Q_{22}Q_{33}-Q_{23}^2\rangle}{\sigma_{11}\sigma_{d1}\sigma_{d2}\sigma_{d3}}\langle|Q_1|\rangle\Phi\left(\frac{\mu}{\sqrt{2}\tau}\right),$$

$$Q_i = \frac{\partial Q}{\partial q_i}, \quad Q_{ij} = \frac{\partial^2 Q}{\partial q_i\partial q_j}. \tag{3.11}$$

where variances σ_{11}, σ_{d1}, σ_{d2}, σ_{d3} are defined by (B4) and (B6) and expressions for $n_{32} = n_{33}$ can be found by cyclic permutation of indices of derivatives Q_i and Q_{ij}.

Functions n_{32} and n_{33} characterize the percolation process in the direction $\boldsymbol{q}_{12}$, and n_{31} characterizes this process in transversal directions. For the most interesting case $q_0 \ll 1$, $q_0 \ll q$ we have

$$l_0^3 n_{32} = l_0^3 n_{33} = n_0\left[\frac{\mu^2}{\tau^2} - \frac{1+2q}{3(1+q)}\right],$$

$$l_0^3 n_{31} = n_0\left(\frac{\mu^2}{\tau^2}-1\right), \tag{3.12}$$

$$n_0 = \frac{3}{4\pi^2}\sqrt{\frac{3}{2}}\left(\frac{\mu}{qq_0}\right)^{3/2}\Phi\left(\frac{\mu}{\sqrt{2}\tau}\right).$$

The function n_{31} is similar to the standard expression for an isotropic Gaussian field (BBKS).

The first zero of Euler characteristic describes approximately the percolation when separate higher peaks are incorporated into a larger (in the limiting case – infinite) structure element (Tomita 1990; Mecke & Wagner 1991). The expressions (3.12) show that in the directions orthogonal to $\boldsymbol{q}_{12}$ the percolation takes place at the 'moment' $\tau = \mu(q)$ whereas along $\boldsymbol{q}_{12}$ it occurs later, at $\tau = \mu(q)\sqrt{3(1+q)/(1+2q)}$. This fact favours two-step percolation and percolation along the pancake surface takes place first. For a given q and τ the ratio $n(>q)/n_{31}$ and $n(>q)/n_{32}$ measure the mean surface of formed pancakes.

Expressions (3.7) and (3.12) show that at small τ percolation takes place for pancakes with $m \approx \langle m\rangle \approx 4\tau^2$. This means that only the highest peaks with $m \geq \langle m\rangle, \mu \geq \tau$ can be considered as discrete objects. The number density of such peaks can be obtained from (3.12), for $\mu/\tau > 1$, as

$$l_0^3 n_{\rm pk}(>q,\tau) = n_0\frac{\mu^2}{\tau^2}. \tag{3.13}$$

Later, when objects with $m \sim 1$ are formed and an essential fraction of matter is concentrated in larger pancakes with $m \sim \langle m\rangle \geq \tau$, the percolation takes place through relatively low mass pancakes with $m \leq \langle m\rangle$. This ideal picture will be however strongly distorted by the matter compression or expansion in transversal directions and by pancake disruption due to the gravitational instability.

3.4 Pancake interaction

An important characteristic of pancake interaction is the two-point PDF which gives the conditional probability to form a pancake with the size q at the moment τ at the distance $\boldsymbol{D}_{\rm sep}$ from a pancake with the size D_1 formed at the moment τ_1. Here we will

restrict our consideration to the simplest case when all three vectors, $\boldsymbol{q}$, $\boldsymbol{D}_1$, and $\boldsymbol{D}_{\rm sep}$ are aligned along the same straight line that is the most interesting case for the small separations. Much more cumbersome case of arbitrary arrangement and/or orientation of these vectors will be considered separately.

In this simplest case the conditional probability to have $\Delta S > q/\tau$ is

$$W_{\rm c}\left(>q,\tau,\frac{D_1}{\tau_1},D_{\rm sep}\right)=0.5\times{\rm erfc}(g_2/\sqrt{2}), \tag{3.14}$$

$$g(x,y,r_s)=\frac{x-r_s y}{\sqrt{1-r_s^2}},\quad g_2=g[\mu(q)/\tau,\mu(D_1)/\tau_1,r_s].$$

The function $\mu(q)$ is given by (3.3) and the coefficient of correlation, $r_s(q,\ D_1,\ D_{\rm sep})$, describing the interaction of two pancakes, can be found in Appendix C (C1). The conditional distribution function of such pancakes can be written as

$$N_{\rm c}\left(\frac{q}{\tau};\frac{D_1}{\tau_1},D_{\rm sep}\right)=\sqrt{\frac{2}{\pi}}\frac{{\rm d}g_2}{{\rm d}q}{\rm e}^{-0.5g_2^2}. \tag{3.15}$$

These relations characterize the parameters of pancakes formed at the moment τ under the condition of a pancake formation at the moment τ_1 with the size D_1 and the separation $D_{\rm sep}$.

The basic relation (3.1) implies that two pancakes with sizes D_1 and D_2 and a separation $|D_{\rm sep}|\le 0.5(D_1+D_2)$ merge together and form a single pancake. For larger separations merging of pancakes can also be considered in the same manner as before, but using the Euler position of the formed pancake

$$r_{\rm pan}=\int_{q_2}^{q_1}\frac{r(q)}{q_{12}}{\rm d}q=\frac{1}{1+z}\left[q_{\rm cent}-B(z)\frac{\Delta\phi_{12}}{q_{12}}\right], \tag{3.16}$$

where $q_{\rm cent}=0.5(q_1+q_2)$ is the Lagrangian position of central point of the pancake and $\Delta\phi_{12}=\phi(q_1)-\phi(q_2)$. As is apparent from (3.16), $r_{\rm pan}$ depends on the potential difference, $[\phi(q_1)-\phi(q_2)]/q_{12}$, and therefore the pancake evolution depends on the potential distribution.

As discussed in Paper I around each pancake there is a potential well with a typical size exceeding the mass m of collapsed pancake by a factor of 1.5–2. The matter infall into these potential wells stimulates merging of pancakes formed with a small separation. For larger separation the influence of this factor decreases progressively and the process of merging becomes (almost) random. These results are consistent with predictions of the adhesion model (Shandarin & Zel'dovich 1989).

The conditional probability that two pancakes with sizes D_1 and D_2 whose separation is $|D_{\rm sep}|\ge 0.5(D_1+D_2)$ merge at the moment τ is defined by the condition

$$r_{\rm pan}(D_1,\tau,q_{\rm cent})=r_{\rm pan}(D_2,\tau,q_{\rm cent}+D_{\rm sep}),$$

and instead of equation (3.3) we have for the probability of merging

$$W_{\rm merg}(D_1,D_2,D_{\rm sep})=\frac{1}{2}{\rm erfc}\left[\frac{\chi(D_1,D_2,D_{\rm sep})}{\tau\sqrt{2}}\right] \tag{3.17}$$

The function $\chi(D_1,\ D_2,\ D_{\rm sep})$ is given by (C6). We can extend applicability of the formula (3.17) for small separations by requiring that

$$W_{\rm merg}(D_1,D_2,D_{\rm sep})=1,\quad |D_{\rm sep}|\le 0.5(D_1+D_2). \tag{3.18}$$

4 PANCAKE EVOLUTION AND FORMATION OF FILAMENTS

Similar technique can also be used to estimate the transversal size, the pancakes compression and/or expansion in transversal directions, and other properties of pancakes. As we are interested in the formation of structure elements with typical sizes $q\gg q_0$ the local description through the deformation tensor cannot be used and the imposed conditions make even approximate description of pancake evolution quite cumbersome (see, e.g., Kofman et al. 1994). The general tendencies and rough characteristics of this evolution can only be outlined. Thus, for example, we can estimate the matter fraction compressed within filamentary-like elements and high-density clumps as of about 50 per cent whereas only ~29 per cent of matter is subjected to 1D compression. This estimate implies that larger pancakes could also incorporate an essential fraction of filaments and clumps.

The formation of filaments as well as pancakes disruption are stimulated by the growth of density in the course of pancakes compression, and therefore, probably, during early evolutionary stages, filaments represent the most conspicuous elements of the structure. As was discussed in Section 3.3, filaments merge to form a joint network. Later, when larger pancakes are formed, the evolution of pancakes becomes slower and disruption of pancakes dominates. These expectations are consistent with the observed and simulated matter distribution. Thus, the conspicuous filaments are seen even at $z=3$ (see, e.g., Governato et al. 1998; Jenkins et al. 1998) whereas disrupted walls dominate at small redshifts (LCRS1; LCRS2; DMRT).

4.1 The characteristics of filament formation

Some approximate characteristics of filament distribution can be obtained by considering the formation of filaments as a sequential matter compression along two principal directions. Such two step compression results in formation of high density 'ridge' surrounded by a lower density anisotropic halo. In a coordinate system with the first and second axes oriented along the directions of maximal and intermediate compressions this process can be approximately described by two equations similar to (3.2):

$$Q(q_{12})=q_{12}/\tau,\quad Q(y_{12})=y_{12}/\tau_{\rm f}. \tag{4.1}$$

Here vectors $\boldsymbol{q}_{12}$ and $\boldsymbol{y}_{12}$ and functions $Q(q_{12})$ and $Q(y_{12})$ describe the deformation along the first and second coordinate axes respectively and additional conditions introduced in (3.2) are assumed to be fulfilled. As was discussed above the matter compression along the second axis is accelerated by the pancake formation and *the function $\tau_{\rm f}(z)$ differs from that given by (2.9).*

Bearing in mind these restrictions we will approximately characterize the probability of filament formation, $W_{\rm cr}^{\rm f}$, for given q and y prior to the 'time' τ and $\tau_{\rm f}$ or for given τ and $\tau_{\rm f}$ with sizes larger then q and y, respectively, as the probability to have $Q(q_{12})/q_{12}\ge Q(y_{12})/y_{12}\ge 1/\tau_{\rm f}$, $Q(q_{12})/q_{12}\ge 1/\tau$:

$$W_{\rm cr}^{\rm f}(>q,\tau,>y,\tau_{\rm f})=1-\frac{1}{8}\left[1+{\rm erf}\left(\frac{\mu(q)}{\sqrt{2}\tau}\right)\right]^3$$
$$-\frac{3}{8}{\rm erfc}\left(\frac{\mu(q)}{\sqrt{2}\tau}\right)\left[1+{\rm erf}\left(\frac{\mu(y)}{\sqrt{2}\tau_{\rm f}}\right)\right]^2. \tag{4.2}$$

The PDF for the filaments, $N_{\rm cr}^{\rm f}$, can be found from (4.2) as

$$N_{\rm cr}^{\rm (f)}(q,\tau,y,\tau_{\rm f}) = \frac{8}{3\pi\tau\tau_{\rm f}}\frac{{\rm d}\mu(q)}{{\rm d}q}\frac{{\rm d}\mu(y)}{{\rm d}y}\exp\left[-\frac{\mu(q)}{2\tau^2}-\frac{\mu(y)}{2\tau_{\rm f}^2}\right] \times\left[1+{\rm erf}\left(\frac{\mu(y)}{\sqrt{2}\tau_{\rm f}}\right)\right], \quad 0<q<\infty,\ \ 0<y<\infty \tag{4.3}$$

More adequate characteristic of filaments is the linear mass density, $m_{\rm f}=\pi qy/4$, defined as a mass per unit length of filament. Both in observed and simulated catalogues filaments usually form a less massive part of structure elements with $m_{\rm f}\ll 1$. For such filaments $q\ll 1$, $\mu(q)\approx\sqrt{q}/2$, $y\ll 1$, $\mu(y)\approx\sqrt{y}/2$ and the PDF $N_{\rm cr}^{\rm f}(m_{\rm f})$ can be found from (4.3) as

$$N_{\rm cr}^{\rm f}(m_{\rm f},\tau,\tau_{\rm f}) \approx \frac{1}{2\pi\langle m_{\rm f}\rangle\sqrt{\xi}}\int_0^\infty\frac{{\rm d}x}{x}{\rm e}^{-\frac{\sqrt{\xi}}{2}(x+1/x)} \tag{4.4}$$

$$\xi=\frac{m_{\rm f}}{\langle m_{\rm f}\rangle},\quad \langle m_{\rm f}\rangle = 4\pi\tau^2\tau_{\rm f}^2.$$

The surface density of spatial distribution of filaments can be obtained using the same technique as in Section 3.3.

4.2 The pancake evolution

The separation of filaments into a special class of structure elements also requires a redefinition of population of 'true' pancakes. Now the probability of 'true' pancake formation defined by conditions $Q(q_{12})/q_{12}\geq 1/\tau$, $Q(y_{12})/y_{12}\leq 1/\tau_{\rm f}$ is:

$$W_{\rm cr}^{(p)}(>q,\tau,<y,\tau_{\rm f}) = \frac{3}{8}{\rm erfc}\left(\frac{\mu(q)}{\sqrt{2}\tau}\right)\left[1+{\rm erf}\left(\frac{\mu(y)}{\sqrt{2}\tau_{\rm f}}\right)\right]^2.$$

instead of expressions (3.2) and (3.3). The PDF for such pancakes is

$$N_{\rm cr}^{(p)}(q,\tau) = \sqrt{\frac{2}{\pi}}\frac{{\rm d}\mu(q)}{\tau{\rm d}q}\exp\left(-\frac{\mu^2}{2\tau^2}\right),\quad 0\leq q\leq\infty. \tag{4.5}$$

$$\langle m_{\rm p}\rangle = 4\tau^2\quad q\ll 1.$$

This PDF differs from (3.6) by the form of the function $\Phi(x)$ what decreases the PDF for larger μ/τ.

As before, expression (4.5) characterizes pancakes by the surface mass density of collapsed matter, q. However, the pancake surface mass density varies with time after pancake formation owing to transversal compression or expansion that results, in particular, in the formation of filaments. Even if these transversal motions do not lead to such dramatic results they can change drastically the *observed* surface density of pancakes. So, the current surface mass density $m_{\rm p}=q/s_{\rm p}$, where $s_{\rm p}$ describes the variation of pancake surface caused by transversal motions, is a more adequate characteristic of pancakes.

As was discussed above this period of pancake evolution is not adequately described by the Zel'dovich theory and our results become unreliable. To obtain qualitative characteristics of influence of these factors we can, for example, describe the variation of the surface of a pancake as

$$s_{\rm p}\propto[1-\tau^*Q(y_{12})/y_{12}][1-\tau^*Q(z_{12})/z_{12}].$$

Here vectors $\boldsymbol{y}_{12}$ and $\boldsymbol{z}_{12}$, and functions $Q(y_{12})$ and $Q(z_{12})$, describe the deformation along the second and third coordinate axes respectively. The function τ^* differs from that given by (2.9) and it can depend on transversal motions. Even so rough consideration shows that the exponential term in (4.5) is eroded, and the resulting PDF becomes power-like:

$$N(m_{\rm p}\ll 1)\propto m_{\rm p}^{-1/2},\quad N(m_{\rm p}\gg 1)\propto m_{\rm p}^{-2}. \tag{4.6}$$

The pancake disruption accelerates this erosion as well and makes the PDF more complicated.

This discussion shows that slowly evolving pancakes with slower transversal motions can be separated into a special subpopulation for which the surface density changes slowly, $m_{\rm p}\approx q$, and the PDF (4.5) correctly describes the pancake distribution during the essential period of evolution. This subpopulation is singled out by conditions

$$|Q(z_{12})/z_{12}|\leq|Q(y_{12})/y_{12}|\leq\epsilon/\tau,\quad \epsilon<1$$

and the probability of existence of such pancakes is proportional to τ^{-2}. This factor describes the disappearance of such pancakes in the course of evolution. This subpopulation can be however quite rich (see the discussion in Section 9).

5 STATISTICAL CHARACTERISTICS OF DARK MATTER STRUCTURE ELEMENTS

Results obtained above allow us to find the approximate PDF and other characteristics of structure elements. The *structure element* with a size (mass) m is defined as a pancake with the size m formed at a moment τ that not merged with any other pancake.

5.1 Merging of dark matter structure elements

As before the characteristics of *structure element* at a moment τ are expressed through characteristics of initial perturbations. The approximate expression for the PDF of structure element can be written in a form similar to the known equation of coagulation

$$N_{\rm str}(m,\tau) = \int_0^\infty{\rm d}y\int_0^m{\rm d}xN_{\rm cr}(x,\tau)N_{\rm c}(m-x,x,y,\tau) \times\frac{{\rm d}W_{\rm merg}(x,m-x,y)}{{\rm d}y} - N_{\rm cr}(m,\tau)\int_0^\infty{\rm d}x\int_0^\infty{\rm d}yN_{\rm c}(x,m,y,\tau)\frac{{\rm d}W_{\rm merg}(x,m,y)}{{\rm d}y}. \tag{5.1}$$

The functions $N_{\rm cr}$, $N_{\rm c}$ and $W_{\rm merg}$ are given by (3.6), (3.15), (3.17) and (3.18). Here the first term describes the formation of two pancakes with sizes x and $m-x$ and a separation y and their merging to a pancake with the size m while the second term describes merging of the pancake of size m with another pancake. If the mass exchanged during merging is incorporated into the forming pancake then the first term in (5.1) has to be appropriately changed.

Here, as the first step of investigation, we will use the simpler approximate approach based on the survival probability of a pancake with size m to avoid merging with larger pancakes with sizes $x\geq m$. For the more interesting case of smaller pancakes with $q_0\ll m\leq x<1$, the most probable process is the formation of two pancakes with sizes m and $x\geq m$ at a small separation $|D_{\rm sep}|\leq 0.5(x+m)$ that means, as follows from (3.1), formation

of one structure element with a size x. This process is described by the second term in (5.1). Because in this case the probability of merging quickly decreases for larger separations $|D_{\rm sep}| \geq 0.5(m+x)$ and the function $W_{\rm c}(m,\ x,\ D_{\rm sep})$ weakly depends on $D_{\rm sep}$, we will use the approximate expression for the probability of merging, $P_{\rm mrg}$,

$$P_{\rm mrg}(m,\tau) \approx 2W_{\rm c}\left(m,\tau,\frac{m}{\tau},\frac{m}{\tau}\right), \tag{5.2}$$

$$P_{\rm mrg}(m,\tau) \approx {\rm erfc}\left[\frac{\mu(m)}{\tau\sqrt{2}}\right],\quad m \ll 1, \tag{5.3}$$

and for the survival probability, $P_{\rm surv}$,

$$P_{\rm surv}(m,\tau) \approx 1 - P_{\rm mrg}(m,\tau), \tag{5.4}$$

$$P_{\rm surv}(m,\tau) \approx {\rm erf}\left[\frac{\mu(m)}{\tau\sqrt{2}}\right],\quad m \ll 1.$$

In spite of the approximate character of this approach, it allows us to obtain reasonable estimates of the expected efficiency of merging and of the large-scale bias. As it is directly seen from (5.4), for $\mu(m) \leq \tau$,

$$P_{\rm surv}(m,\tau) \propto \mu(m)\tau^{-1},$$

what characterizes the impact of pancake merging.

5.2 Statistical characteristics of structure elements

With this survival probability the approximate PDF for the structure elements, $N_{\rm str}(q,\tau)$, can be written as follows

$$N_{\rm str}(m,\tau) \propto P_{\rm surv}(m,\tau)N_{\rm cr}(m,\tau). \tag{5.5}$$

These relations allow us to obtain also the approximate mass distribution function, $N^{(\rm m)}_{\rm str}(m,\tau)$, characterizing the distribution of compressed matter over the structure elements. For the more interesting case $m \ll 1$ we have

$$N_{\rm str}(m,\tau) \approx \frac{24}{17\sqrt{2\pi}\tau}\frac{{\rm d}\mu}{{\rm d}m}\Phi\left(\frac{\mu}{\sqrt{2}\tau}\right){\rm erf}\left(\frac{\mu}{\sqrt{2}\tau}\right), \tag{5.6}$$
$$\langle m\rangle \approx 8\tau^2.$$

In the general case this function can be obtained numerically. The mean cumulative comoving linear number density of structure elements, $n_{\rm str}(>m,\tau)$, is

$$n_{\rm str}(>m,\tau) \approx -\int_m^\infty {\rm d}m\frac{{\rm d}n(>m,\tau)}{{\rm d}m}P_{\rm surv}(m,\tau)$$

$$= n(>m,\tau)P_{\rm surv}(m,\tau) + \int_m^\infty {\rm d}m n(>m,\tau)\frac{{\rm d}P_{\rm surv}(m,\tau)}{{\rm d}m}. \tag{5.7}$$

Some of these functions are plotted in Figs 1, 2 and 3. Fig. 1 shows the PDF, $N_{\rm str}(m,\tau)$, the mass function, $mN_{\rm str}(m,\tau)$, and the cumulative mass function, $f(>m)$, for structure elements versus the $m/m_{\rm m}$ for five time moments. Here $m_{\rm m}$ is the median mass of structure elements defined by the condition $f(>m_{\rm m}) = 0.5$. At small τ the distribution function is rapidly changing owing to the merging of smaller pancakes. Later the evolution is slower and it is sustained by growth of median mass owing to the progressive matter concentration within richer structure elements.

The same effect is clearly seen in Fig. 2 where the mean linear number density of structure elements, $l_0 n_{\rm str}(>m,\tau)$, is plotted for the same time moments. Rapid merging of low-mass pancakes and formation of more massive pancakes changes the shape of this function at $m \ll m_{\rm m}$ and $m \gg m_{\rm m}$ while at $m \sim m_{\rm m}$ evolution is very slow. The function $D_{\rm str}(f)$ plotted in Fig. 2 (bottom panel) is similar to that found in simulations (DFGMM).

Time dependence of the mean, $\langle m\rangle$, and median, $m_{\rm m}$, masses of structure elements is plotted in Fig. 3 (top panel) together with fits

$$\langle m(\tau)\rangle \approx 9\tau^2/(1+4\tau),\quad \tau \leq 1.5, \tag{5.8a}$$

$$m_{\rm m}(\tau) \approx 0.03 + 2.2\tau,\quad \tau \leq 1.5. \tag{5.8b}$$

Faster growth of $\langle m(\tau)\rangle$ in comparison to (3.7) is caused by merging of pancakes as it is described by (5.5). In Fig. 3 (top panel) the $D_{str}(m_m,\tau)$ is plotted together with the fit

$$D_{\rm str}(m_{\rm m},\tau) \approx 1.5 \times l_0\sqrt{\frac{\tau}{\tau+0.07}} \tag{5.8c}$$

The bottom panel in Fig. 3 shows evolution of the linear number density of structure elements, $l_0 n$, caused by their exponentially fast formation at smaller τ, and later, by successive merging which is well fitted by the expression $D_{\rm str}(>q,\tau) \propto \tau^{-0.4}$ which is slower than that found in DFGMM.

5.3 Parameters of structure in observed catalogues

In previous sections the formation and evolution of structure was described in a comoving space. However, in observed catalogues the redshift position of galaxies along the line of sight is used. This difference distorts the parameters of observed structure with respect to the theoretical expectations (see, e.g., Melott et al. 1998; Hui, Kofman & Shandarin 1999). To take into account this distortions the theoretical relations given above need to be modified.

In observational catalogues the distance to a galaxy is defined by its observed velocity which can be found from (2.1) as

$$v_i = \frac{H(z)}{1+z}[q_i - \beta(z)B(z)S_i(\boldsymbol{q})],$$

$$\beta = 1 - \frac{1+z}{B}\frac{{\rm d}B(z)}{dz},\quad 1 \leq \beta \leq 2, \tag{5.9}$$

where $H(z)$ is the Hubble constant. Therefore, for observed catalogues all relations obtained above will be valid after replacement

$$\tau(z) \rightarrow \tau_v(z) = \tau(z)[\beta(z)\cos\varphi + \sin\varphi], \tag{5.10}$$

where φ is a random angle between the line of sight and the direction of pancake compression. It is evident that $1 \leq \tau_v/\tau \leq \sqrt{\beta^2+1}$, and for $\varphi = \pi/2$, $\tau_v = \tau$. This means that the observed structure parameters will be randomly increased with respect to those found in the comoving space.

The value of this distortion depends on the cosmological parameters and redshift and is superposed with distortions generated by the structure disruption, selection effects, and other random factors. The well-known example of such distortion is the effect of so called 'Finger of God'. The direct comparison of simulated structure parameters in comoving and redshift spaces performed in DMRT demonstrates a moderate dependence of the main structure properties on these factors. But some properties of

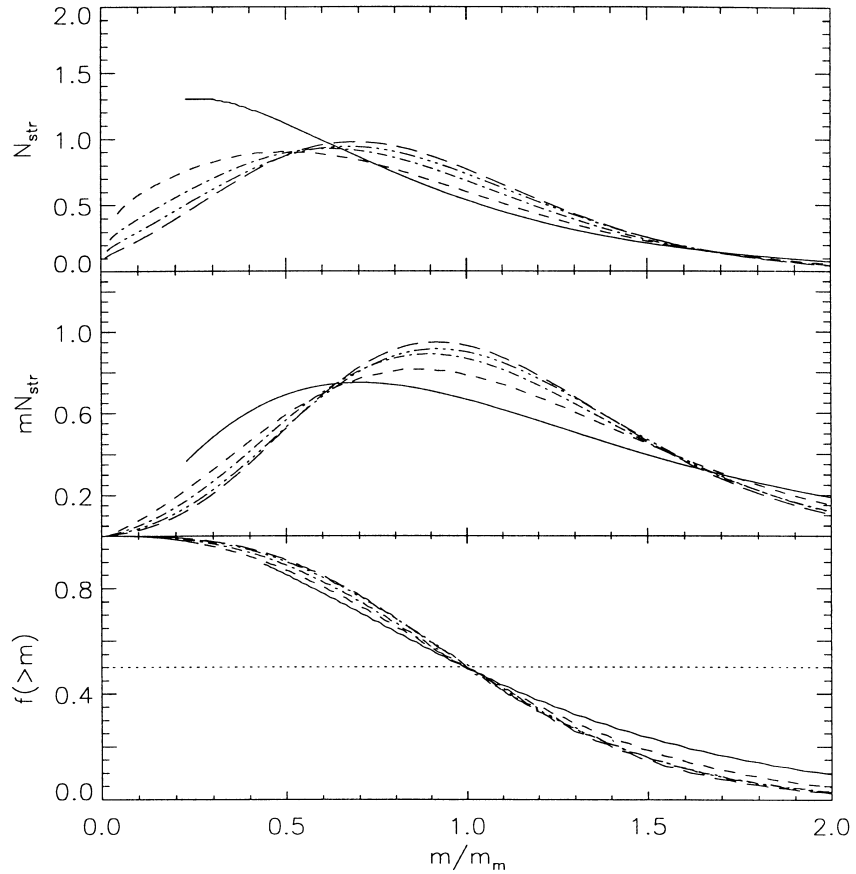

Figure 1. The PDF of structure elements, $N_{\rm str}(m,\tau)$, the mass distribution function, $mN_{\rm str}(m,\tau)$, and the fraction of compressed matter, $f(>m)$, versus the masses (sizes) of structure elements, $m/m_{\rm m}$, are plotted for five moments of time: $\tau = 0.1$ (solid line), $\tau = 0.3$ (dashed line), $\tau = 0.5$ (dot-dashed line), $\tau = 0.7$ (dot-dot-dot-dashed line), $\tau = 2$ (long-dashed line).

the structure such as characteristics of galaxy distribution within walls are different in comoving and redshift spaces. More details can be found in Section 9 and DMRT.

6 FORMATION OF VOIDS

The same method can be used to solve the complementary but more complicated problem of void formation. According to the Zel'dovich theory the probability to find a 'void' with a size $r > r_v$ is identical to the probability that the inequality

$$(1+z)r = q_1 - q_2 - \tau\Delta S_{12} \geq (1+z)r_v \tag{6.1}$$

holds under the conditions that pancakes have been formed near the boundary points q_1 and q_2, and in the absence of any pancakes between points q_1 and q_2. This is equivalent to the probability that the inequality

$$\Delta S_{12} \leq [q_{12} - (1+z)r_v]/\tau \tag{6.2}$$

holds under the same conditions.

More accurately we can consider the *underdense regions* bounded by pancakes with masses m_1 and m_2 (or with masses exceeding the threshold mass, m_1, $m_2 \geq m_{\rm thr}$) in the absence of any pancakes with masses $m \geq m_{\rm thr}$ between points q_1 and q_2. The methods discussed above and supplemented by the void probability function technique could be used, in principle, to obtain such a probability but the derivation becomes very cumbersome owing to many additional conditions. Numerical methods similar to that used by Sahni, Sathyaprakash & Shandarin (1994) could be more suitable for such an investigation.

Let us remind however that the parameters of under dense regions are closely linked to the spatial distribution of initial gravitational potential what allows to specify conveniently the large-scale perturbations. This link is clearly demonstrated by the adhesion approach (see, e.g., Shandarin & Zel'dovich 1989) and was discussed in detail in Paper I. It can also be described with the technique considered above. Thus, for example, the large-scale modulation of the pancake distribution by the spatial distribution of this potential can be described as a modulation of the effective 'time' moment $\tau_{\rm eff}$.

To illustrate this statement we can consider the pancake formation for a given potential difference, $\Delta\phi$, between two points with comoving coordinates x_1 and $x_1 + D_{\rm cell}$. In this case the distribution function of the pancake with a size $m \ll D_{\rm cell}$ at the point with a comoving coordinate $x_1 \leq y \leq x_1 + D_{\rm cell}$ is given by (3.6) and (5.5) with

$$\frac{1}{\tau_{\rm eff}(x)} \approx \frac{1}{\tau}\left[1 - \kappa_\phi(D_{\rm cell}, y)\frac{\Delta\phi}{\sigma_\phi}\right], 0 \leq y \leq D_{\rm cell},$$

$$\sigma_\phi^2 = 2G_0(D_{\rm cell}), \quad \kappa_\phi = G_{12}(y) - G_{12}(D_{\rm cell} - y). \tag{6.3}$$

Here σ_ϕ is the dispersion of gravitational potential difference at the points with the separation $D_{\rm cell}$. Functions G_0 and G_{12} are introduced in Appendix A.

As is seen from (6.3) the efficiency of pancake formation

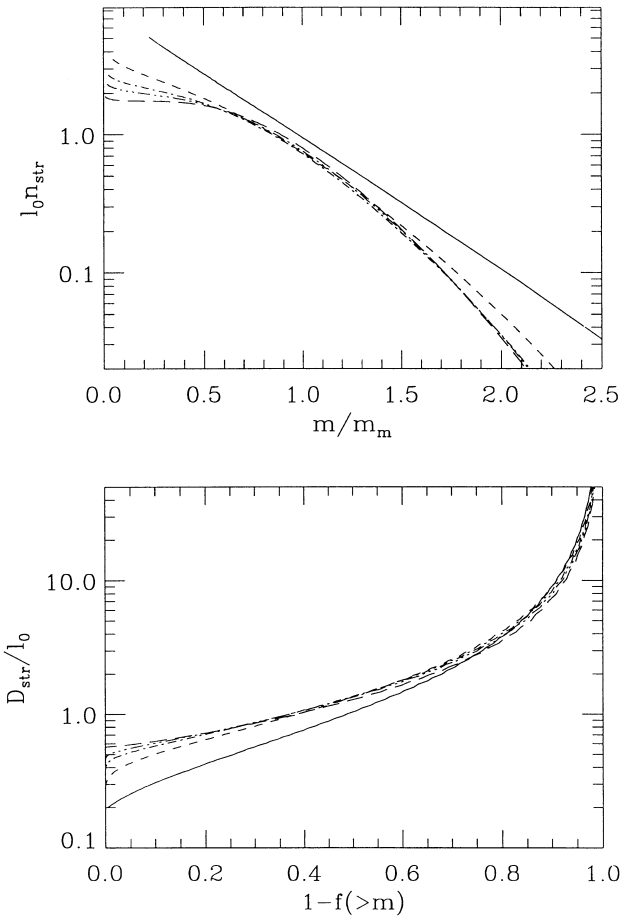

Figure 2. Top panel: the mean comoving linear density of a pancake, $l_0 n_{\rm str}(>m,\tau)$, versus masses $m/m_{\rm m}$ are plotted for five moments of time: $\tau = 0.1$ (solid line), $\tau = 0.3$ (dashed line), $\tau = 0.5$ (dot-dashed line line), $\tau = 0.7$ (dot-dot-dot-dashed line), $\tau = 2$ (long-dashed line). Bottom panel: the mean separations of pancakes, $D_{\rm str}(> m,\tau)/l_0$, versus the fraction of compressed matter $f(> m)$, for the same time moments.

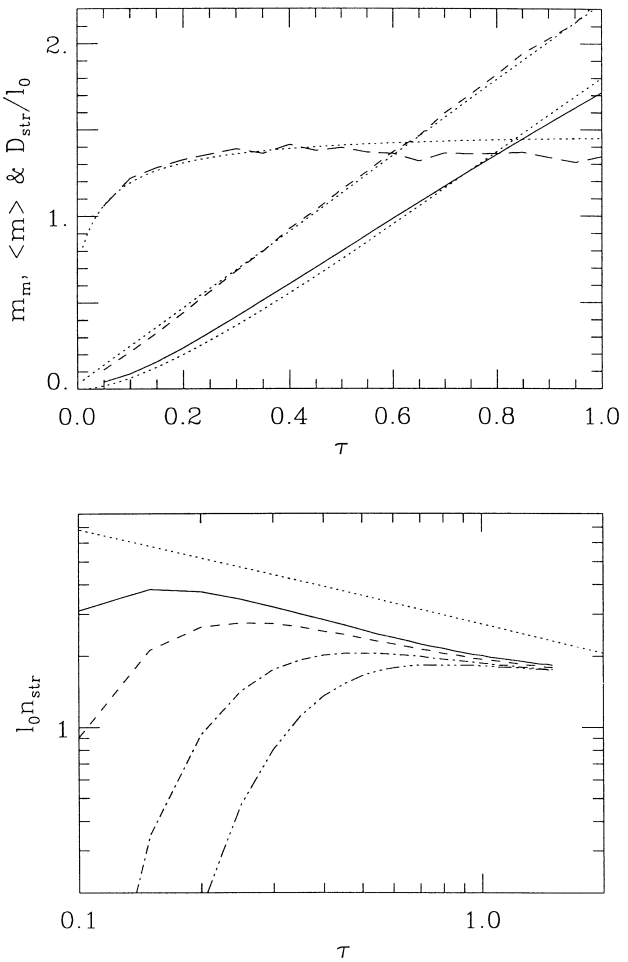

Figure 3. Top panel: time dependence of the mean mass, $\langle m\rangle$, (solid line), median mass, $m_{\rm m}$, (dashed line) and the mean separation $D_{\rm sep}(m_{\rm m})/l_0$. The fits (5.8) are plotted by dotted lines. Bottom panel: evolution of the mean comoving linear number density of structure elements, $n_{\rm str} l_0$, versus τ for four threshold masses $m/l_0 \geq 0.05$ (solid line), $m/l_0 \geq 0.1$ (dashed line), $m/l_0 \geq 0.3$ (dot-dashed line), $m/l_0 \geq 0.5$ (dot-dot-dot-dashed line). A power law $\tau^{-0.4}$ is plotted by a dotted line.

depends directly on the coordinate y and the potential difference, $\Delta\phi(D_{\rm cell})$. It is amplified in regions with $\kappa_\phi \Delta\phi \leq 0$, and depressed in regions with $\kappa_\phi \Delta\phi \geq 0$.

The same large-scale modulation modifies the Euler position of pancake and instead of equation (3.16) we obtain after averaging of $\Delta\phi(m)/m$ (under the condition $m \ll D_{\rm cell}$)

$$\langle (1+z) r_{\rm pan}\rangle = y + \tau G_r(y, D_{\rm cell}) \frac{\Delta\phi}{\sigma_\phi},$$

$$G_r(y,D) = y G_{12}(y) + (D-y) G_{12}(D-y), \tag{6.4}$$

and for the mean Eulerian linear number density of pancakes

$$n_{\rm e}(y) = \left(\frac{\partial r_{\rm pan}}{\partial y}\right)^{-1} = \frac{1+z}{1+\tau G_n(y, D_{\rm cell}) \dfrac{\Delta\phi}{\sigma_\phi}}, \tag{6.5}$$

$$G_n(y,D) = G_{12}(y) - G_{12}(D-y) + y^2 G_{23}(y) - (D-y)^2 G_{23}(D-y).$$

These expressions describe the matter infall into wells of initial gravitational potential and clearly demonstrate the close connection of under dense regions with the spatial distribution of initial gravitational potential. More detailed discussion of this effect can be found in Paper I.

7 LARGE-SCALE BIAS AND CHARACTERISTICS OF BIASED COLD MATTER DISTRIBUTION

7.1 Large-scale bias

In observations we have to deal with the galaxy distribution which is, probably, biased relative to the spatial distribution of dark matter in the considered range of scales. The qualitative physical ground of such large-scale bias is transparent and was discussed already 10 years ago by Dekel & Silk (1986), and Dekel & Rees (1987). It can be caused by the joint action of large-scale perturbations and reheating of the baryonic component of matter. The interaction of large- and-small scale perturbations shows up as an excess of low-mass pancakes and acceleration of their growth within richer wall-like elements and is seen in simulations as a strong concentration of high density peaks within filaments and richer walls. It results in an excess of compressed cold gas inside 'proto' walls before reheating. However, after reheating further compression and cooling of gas are inhibited owing to the

growth of entropy of uncompressed gas. This excess of *cold, low-entropy baryonic matter*, reached at the reheating redshift, $z = z_h$, can be considered as the excess of galaxies within richer walls that is the large-scale bias in spatial galaxy distribution.

In Paper I the modulation of the rate of pancake formation by the large-scale perturbations of initial gravitational potential was discussed. Here we consider the direct interaction of earlier and later pancakes, that allows us to obtain more reliable estimates of the large-scale bias. With the technique developed above we can consider only the direct interaction of two population of pancakes, namely, those created at $z = z_h$, and at $z = 0$, and we have to neglect the mutual influence of intermediate population of pancakes accumulated by the walls. Such an influence can in principle be considered but the description becomes very cumbersome. So, our estimate presented below is actually the lower limit of the possible large-scale bias. Perhaps, this problem can be studied in simulations which take into account all important factors together (see, e.g., Sahni, Sathyaprakash & Shandarin 1994; Cole et al. 1998).

For the warm dark matter model discussed in Paper I the mass of DM particles restricts the minimal size of created pancakes to the correlation scale of initial density perturbations, r_c. For the CDM power spectrum considered here there are no natural limits and, in principle, pancakes with arbitrarily low mass can form. Formally, it is due to the divergence of higher moments of power spectrum and, because of this, the typical scale r_c is zero. In this case, however, the typical scale q_0 introduced by (3.4) plays similar role and discriminates the process of earlier low-mass pancake formation, described through the deformation tensor, and later formation of structure elements discussed above. The typical mass of such low-mass pancakes given by the expression (3.4) exceeds the estimates of minimal baryonic mass formed before the reheating, $M_{\min} \sim 10^6\ \mathrm{M}_\odot$ (Tegmark et al. 1997), and the value q_0 can be accepted as a natural limit of pancake size. Further evolutionary history of low-mass pancakes is uncertain, and this problem should be considered separately.

Thus, for the CDM power spectrum we assume that:

(i) all baryons accumulated by structure elements with a size $m \geq q_0$, at the redshift $z = z_h$, $\tau = \tau_h$, are incorporated into observed 'galaxies';

(ii) the formation of such clouds is interrupted at the redshift $z = z_h$, $\tau = \tau_h$ by the instantaneous reheating of the uncompressed gas.

Both assumptions are very restrictive but they can be used for rough estimates of the efficiency of this mechanism of generation of the large-scale bias. The moment of reheating is, probably, restricted to $7 \leq z_h \leq 15$. The lower limit is imposed by the observational constrains. The upper limit is imposed by the very fast growth of the inverse Compton cooling for larger redshifts.

This means that for the models with $\Omega_m \sim 0.3$–1 the reheating probably occurred at $\tau_h = \tau(z_h) \approx (0.15\text{–}0.3)\tau_0$.

7.2 Statistical characteristics of biased cold matter distribution

The biasing factor on the LSS and SLSS scales can be estimated in the same manner as the probability of merging (5.2). Now we are interested in the mass of cold matter collapsed at $\tau = \tau_h$ which was accumulated at the moment τ by a pancake with a size $D \gg m_{\mathrm{cld}}$. The approximate PDF for this mass can be written as

$$N_{\mathrm{cld}}(m_{\mathrm{cld}}, \tau_h) \approx 2N_c\left(m_{\mathrm{cld}}, \tau_h; D, \tau, \frac{m_{\mathrm{cld}} + D}{2}\right)$$

$$\approx N_{\mathrm{cr}}(m_{\mathrm{cld}}, \tau_1), \tag{7.1}$$

$$\frac{1}{\tau_1} = \frac{1}{\tau_h} - \frac{\kappa_1(D)}{\tau}, \quad \kappa_1(D) \approx \frac{1}{(2+D)(1+D)}.$$

These relations show that, as it was discussed in Paper I, the formation of earlier pancakes within larger structure elements is accelerated, what is seen in (7.1) as a shift of the effective evolutionary 'time', τ_1, relatively to the real reheating 'time' moment, τ_h. The corresponding mean 'mass' of such pancakes can be found as

$$\langle m_{\mathrm{cld}}(\tau_h)\rangle \approx 4\tau_1^2 \approx 4\tau_h^2(1 + 1.5\tau_h/\tau), \quad D < 1. \tag{7.2}$$

The dimensionless biasing factor

$$b_{\mathrm{bias}} = \frac{\langle m_{\mathrm{cld}}\rangle}{\langle m\rangle} - 1 \approx 1.5\tau_h/\tau, \tag{7.3}$$

is about of 1/5–2/5 and weakly depends on the size D of the considered structure element. The relation (7.1) describes also the excess of larger pancakes induced by the influence of larger structure elements

$$\frac{N_{\mathrm{cld}}(m_{\mathrm{cld}}, \tau_h)}{N_{\mathrm{cr}}(\mu, \tau_h)} \approx \frac{\tau_h}{\tau_1}\exp\left(\frac{m_{\mathrm{cld}}}{2\tau_h\tau}\right). \tag{7.4}$$

As is seen from (7.1) the bias decreases, for $\tau \gg \tau_h$. This means that the indirect multi step interaction becomes specially important and the intermediate population of pancakes formed at $\tau_h \leq \tau^* \leq \tau$ with a size $x^* \leq D$ and accumulated by a structure element with a size D, at the moment τ, will enhance the bias and increase the concentration of cold matter within larger pancakes.

These results are consistent with the conclusions of Paper I, Cole et al. (1998) and Sahni, Sathyaprakash & Shandarin (1994) and demonstrate the sensitivity of the considered bias to the detailed characteristics of the process of galaxy formation. They show that the overdense and underdense regions found now in the observed galaxy distribution can, probably, be related even at high redshifts to a spatial modulation of sizes of the earlier pancakes. The larger pancakes are more closely associated with overdense regions whereas the underdense regions are occupied preferentially by low-mass pancakes.

Summarizing, we can infer that the influence of large-scale bias generated by a combined action of reheating and large-scale perturbations can be important and can distort characteristics of the observed galaxy distribution relative to the same characteristics of DM distribution. Under suitable conditions the fraction of baryons accumulated by galaxies can be suppressed in low-mass pancakes and underdense regions and increased in richer structure elements.

8 DYNAMICAL CHARACTERISTICS OF THE PANCAKES

In this section we will find two dynamical characteristics of pancakes, namely, the velocity of pancakes as a whole and the dispersion of matter velocity within pancakes caused by compression of pancakes.

The velocity of an infalling particle, v_i, can be found from (2.1) as

$$v_i(\boldsymbol{q},z) = \mathrm{d}r_i/\mathrm{d}t = \frac{H(z)}{1+z}[q_i - \beta(z)B(z)S_i(\boldsymbol{q})], \tag{8.1}$$

$$\beta = 1 - \frac{1+z}{B}\frac{\mathrm{d}B(z)}{\mathrm{d}z},$$

where $H(z)$ is the Hubble constant.

The functions $\beta(z)$ can be found from (2.2) and (2.3) as

$$\beta \approx 2 - B^3(z)\frac{1-\Omega_\mathrm{m}}{1+1.2\Omega_\mathrm{m}}, \quad \Omega_\mathrm{m} + \Omega_\Lambda = 1, \tag{8.2}$$

$$\beta \approx 2 - B(z)\frac{1-\Omega_\mathrm{m}}{1+1.5\Omega_\mathrm{m}}, \quad \Omega_\mathrm{m} \le 1, \quad \Omega_\Lambda = 0. \tag{8.3}$$

For $\Omega_\mathrm{m} = 1$ both expressions give $\beta = 2$.

Using the general relation for the velocity of a particle (8.1) we can find the velocity of a pancake as a whole through the momentum conservation law, we have

$$v_\mathrm{pan} = \frac{1}{q_{12}}\int_{q_2}^{q_1} v(q)\mathrm{d}q = \frac{H(z)}{1+z}\left[q_\mathrm{cent} - \beta B(z)\frac{\Delta\phi_{12}}{q_{12}}\right],$$

$$\Delta\phi_{12} = \phi(q_1) - \phi(q_2), q_\mathrm{cent} = (q_1+q_2)/2. \tag{8.4}$$

The pancake position, r_pan, was given by (3.16). The peculiar velocity of pancake is

$$u = v_\mathrm{pan} - H(z)r_\mathrm{pan} = \frac{H(z)}{1+z}B(\beta-1)\frac{\Delta\phi_{12}}{q_{12}}. \tag{8.5}$$

The mean peculiar velocity, $\langle u\rangle = 0$, and its dispersion, σ_u, is

$$\sigma_u^2(z) = \frac{H^2(z)}{(1+z)^2}[\beta(z)-1]^2B^2(z)\frac{2G_0(q_{12})}{q_{12}^2}. \tag{8.6}$$

The distribution function of peculiar velocity is Gaussian as before. In dimensional variables, at $z = 0$, and for $q_{12} \ll 1$, we have:

$$\sigma_u(0) = H_0[\beta(0)-1]\sigma_s/\sqrt{3} = H_0[\beta(0)-1]l_0\tau_0. \tag{8.7}$$

These relations show that for smaller q_{12} the velocity of the pancakes is close to the mean velocity dispersion and decrease $\propto q_{12}^{-1/2}$, for $q_{12} > 1$. The vortexless character of the initial velocity perturbations is clearly seen in equations (8.4) and (8.5).

Variations of the pancake velocity with the transversal coordinates can distort the shape of pancake and, in principle, can destroy the pancake. The impact of this factor can be characterized through the expression (8.4) as a correlation of pancake velocity at different transversal coordinates. This correlation is described by the normalized function r_v (see Appendix D), and for $q_{12}, q_{34} \ll 1$, we have

$$r_v = \boldsymbol{q}_{12}\cdot\boldsymbol{q}_{34}/q_{12}q_{34}, \tag{8.8}$$

that demonstrates the regular character of velocity variations. For larger q_{12} and q_{34} the velocity dispersion (8.6) decreases and therefore this factor becomes less important.

The velocity dispersion within a pancake with a given mass $q = q_1 - q_2$, caused by the matter infall into pancake, is defined by the energy conservation law. The velocity of a particle with the coordinate q_3 relative to the pancake as a whole is

$$v_\mathrm{inn}(q_3,z) = v(q_3,z) - v_\mathrm{pan}(z) = \frac{H(z)}{1+z}\left[q_3 - q_\mathrm{cent} - \beta(z)B(z)\left(S(q_3) - \frac{\Delta\phi_{12}}{q_{12}}\right)\right]. \tag{8.9}$$

Using the conditional mean values and dispersions of random functions $S(q_3)$, and $\phi(q_1) - \phi(q_2)$, listed in Appendix A, we obtain the required velocity dispersion

$$\frac{(1+z)^2}{H^2(z)}\sigma_v^2 = \frac{q^2}{12}[(\beta(z)-1)^2 + 2\beta(z)f_1(q) - \beta^2(z)f_2(q) + \tau^2\beta^2(z)f_3(q)]. \tag{8.10}$$

The functions f_1, f_2 and f_3 are given in Appendix D. The velocity dispersion $\sigma_v(q)$ is plotted in Fig. 4 for a few cosmological models, for $z = 0$, $h = 0.7$.

For $q_{12} \le 1$ the functions f_1, f_2 and f_3 are small, $f_1 \le 0.06$, $f_2 \le 0.13$ and $f_3 \le 0.2$, and the contribution of the three last terms in (8.9) becomes important only when $\beta \sim 1$ that is for cosmological models with a lower matter density at redshift $z \le 1$. For poorer pancakes, the simple approximate relation

$$\sigma_v^2 \approx \frac{H^2(z)}{(1+z)^2}\left[(\beta-1)^2\frac{q_{12}^2}{12} + \tau^2\beta^2\frac{q_{12}}{3}\right] \tag{8.11}$$

can be used for estimates of the expected velocity dispersion. For such pancakes the distribution function of σ_v is similar to (4.5).

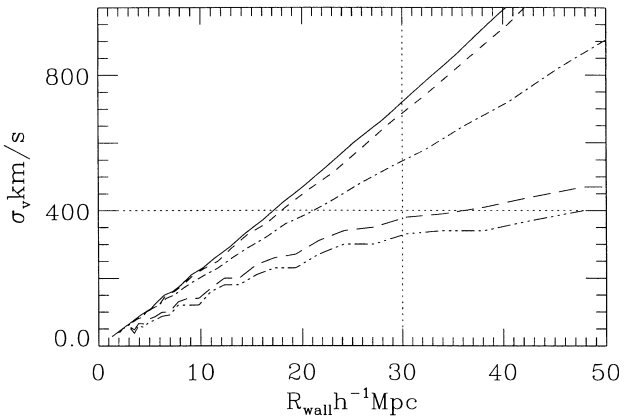

Figure 4. The velocity dispersion, σ_v, versus the size of 'proto walls', $q = R_\mathrm{wall}$, for the redshift $z = 0$, for five cosmological models with $h = 0.5$, $\Omega_\mathrm{m} = 1, \Omega_\Lambda = 0$ (solid line), and $h = 0.7$, $\Omega_\mathrm{m} = 0.5$, $\Omega_\Lambda = 0.5$ (dashed line), $\Omega_\mathrm{m} = 0.5$, $\Omega_\Lambda = 0$ (dot-dashed line), $\Omega_\mathrm{m} = 0.35$, $\Omega_\Lambda = 0.65$ (dot-dot-dot-dashed line), $\Omega_\mathrm{m} = 0.3$, $\Omega_\Lambda = 0$ (long-dashed line). Dotted lines show observational estimates of the size of 'proto walls' $R_\mathrm{wall}\sim 30h^{-1}$ Mpc, and the velocity dispersion $\sigma_v \sim 400\,\mathrm{km\,s^{-1}}$.

9 COMPARISON WITH SIMULATED AND OBSERVED STRUCTURE PARAMETERS

Some characteristics of large-scale galaxy distribution can be extracted from available catalogues of galaxies and clusters of galaxies and catalogues of absorbers in spectra of quasars. Some characteristics of large-scale DM distribution can be derived from available simulations. All these characteristics are distorted by

selection effects, bias between spatial distribution of DM and galaxies, and other factors which complicate the direct comparison of characteristics obtained with different methods and data bases.

Nonetheless, the comparison of even so distorted characteristics with the expected characteristics discussed above can be interesting as it allows one to compare various estimates and illustrates their sensitivity to basic cosmological parameters and other factors. More detailed discussion can be found in DMRT and LCRS2.

9.1 Observed and simulated parameters of the structure

Analysis of galaxy distribution in the Las Campanas Redshift Survey (Shectman et al. 1996) shows that the richer and poorer structure elements can be assigned to wall-like and filamentary populations, but the accurate demarcation of these subpopulations is problematic. Both subpopulations accumulate ≈ 40–60 per cent of galaxies. Filaments fill the gaps between the walls and form a random network with the mean cell size $D_{\rm f}^{\rm obs} \sim 10$–$12h^{-1}$ Mpc at $z = 0$. The richer walls can be formed owing to an anisotropic compression of matter within slices with a typical size of $R_{\rm wall}^{\rm obs} \approx 20$–$25h^{-1}$ Mpc and with a typical separation of $D_{\rm wall}^{\rm obs} \sim 50$–$60h^{-1}$ Mpc (LCRS1 and LCRS2). The walls are significantly disrupted by the small scale clustering of galaxies (see, e.g., fig. 5 in Ramella, Geller & Huchra 1992). The velocity dispersion within such wall-like elements was estimated as $\sigma_v^{\rm (obs)} \sim 350$–$400\,{\rm km\,s^{-1}}$ (Oort 1983a). The bulk velocities of galaxies are now estimated as $\sigma_u^{\rm obs} \sim 400\,{\rm km\,s^{-1}}$ (see, e.g., Dekel 1997). The observed surface density of structure elements is heavily distorted by the selection effects and small-scale clustering and is equally well fitted to a power law, exponential distribution, and functions discussed in Sections 4 and 5.

The structure in the DM distribution was simulated and analysed by DMRT for the SCDM model with $\Omega_{\rm m} = 1$, $h = 0.5$, ΛCDM model with $\Omega_{\rm m} = 0.35$, $\Omega_\Lambda = 0.65$, $h = 0.7$ and OCDM model with $\Omega_{\rm m} = 0.5$, $h = 0.6$. For all these models the normalization to the two-year COBE data were used. These simulations reproduce the structure with the main parameters similar to those found in observations. The analysis shows that walls accumulates ~ 40 per cent of DM with a mean size of 'proto walls' $R_{\rm wall}^{\rm sim} \sim 15 - 20h^{-1}$ Mpc and with a mean separation of walls and filaments $D_{\rm wall}^{\rm sim} \sim 50 - 70h^{-1}$ Mpc, $D_{\rm f}^{\rm sim} \sim 9 - 14h^{-1}$ Mpc, respectively.

In all the models the simulated velocity dispersion within walls, $\sigma_v^{\rm sim}$, is the same along all three principal directions of walls and it is generated by the wall curvature and disruption into a system of high-density clumps. The walls are seen usually as ordered sets of irregular high-density clumps connected by lower density bridges. The degree of wall disruption depends on the code used and reached resolution, and it is more conspicuous in the models with larger $\Omega_{\rm m}$. In the redshift space this inner structure is partly eroded and characteristics of DM walls are similar to that found for the observed galaxy distribution.

The isotropy of simulated velocity dispersion σ_v confirms the essential influence of small-scale clustering on the properties of both observed and simulated structure elements. The instability of a thin compressed layer was analysed in the linear approximation by Doroshkevich (1980) and Vishniac (1983), and was recently simulated by Valinia et al. (1997). The clustering rate and parameters of formed clusters depend on the density of compressed matter and properties of transversal velocity field.

9.2 Comparison of simulated and expected structure properties

Theoretical parameters of DM wall-like structure elements are listed in Table 1 for the median mass $m = m_{\rm m}$ and for $l_{\rm c}/l_0 = 0.056$. The variations of $R_{\rm wall}$ listed in Table 1 are moderate and, in the range of precision of our approximate consideration, these values are similar to those observed and simulated. The differences become more significant only for the OCDM models. The value of $D_{\rm str}$ is sensitive to the assumed mass threshold (see Figs 2 and 6) and can be adjusted.

The simulated structure elements are also distorted by the small-scale clustering but owing to the rich statistics of such elements a more detailed quantitative comparison of simulated and expected properties of the structure can be performed. To do this we will consider the PDFs (4.4) and (4.5) for the surface density of filaments and pancakes, the PDFs for velocity u and velocity dispersion σ_v and direct estimates of important parameters

$$\tau_u = \frac{\sqrt{\langle\sigma_u^2\rangle}}{H_0 l_0(\beta - 1)}, \quad m_v/l_0 = \frac{2\sqrt{3\langle\sigma_v^2\rangle}}{H_0 l_0(\beta - 1)}, \tag{9.1}$$

following from relations (8.7) and (8.11).

To characterize the filamentary and wall-like subpopulations of structure separately the analysis was performed both in the comoving and redshift spaces for three subsamples of structure elements. The first contained all particles, the second and third incorporated the richer and poorer structure elements with $N_{\rm mem} > 200$ and $N_{\rm mem} < 200$, respectively. Here $N_{\rm mem}$ is the number of DM particles within a structure element bounded by the threshold density $n_{\rm thr}/\langle n\rangle = 1.7$, 1.1 and 1.1 for the SCDM, OCDM and ΛCDM models. In all the cases the second subsamples accumulates ~ 40–45 per cent of particles.

To obtain the required PDF a set of rectangular sampling cores was prepared and the number of DM particles in the intersection of separate structure elements with these cores was taken as a characteristic of surface density of structure elements. For each of the cluster its velocity u and velocity dispersion σ_v along the core were also found. To depress the impact of small-scale clustering the analysis was performed for the core size $L_{\rm core} = 10h^{-1}$ Mpc, for the second subsample, and for $L_{\rm core} = 4h^{-1}$ Mpc, for the first and third subsamples when the core size is restricted by the separation of filaments. The random intersection of cores and structure elements generates significant excess of poorer clusters. To depress this effect poorer clusters were rejected and the truncated PDFs were considered. Even so, the number of clusters used was ~ 3500, for the second, and $\sim 10\,000$, for the first and third subsamples. The random orientation of structure elements and cores increases the measured surface density (by a factor of 2 for homogeneous matter distribution, Kendall & Moran 1963), and reduces the measured velocity of structure elements along the core, $u_{\rm c}$, by a factor of $\sqrt{3}$ and we have

$$u_{\rm c} = u\cos\varphi, \quad \tau_u = \sqrt{3}\tau_{u{\rm c}}. \tag{9.2}$$

To compare the simulated and theoretical PDFs the two parameters fits were used. For the second subsample the

Table 1. Main expected parameters of the SLSS.

Ω_m	Ω_Λ	h	l_0 h^{-1}Mpc	τ_0	R_{wall} h^{-1}Mpc	D_{str} h^{-1}Mpc	τ_u	m_v/l_0	τ_v	m_p/l_0	τ_p
1	0	0.5	13.2	0.7	~20.7	~19.8	0.52	1.2	0.42	1.0	0.41
0.5	0.5	0.7	18.9	0.6	~25.5	~26.8					
0.5	0	0.6	22.0	0.3	~14.5	~26.9	0.28	0.5	0.27	0.4	0.29
0.35	0.65	0.7	26.9	0.4	~23.5	~37.1	0.40	0.9	0.36	0.7	0.37
0.35	0	0.7	26.9	0.2	~12.0	~34.5					

distribution of surface density was fitted to the expression

$$N_w = \frac{a_w}{\sqrt{x_w}} e^{-x_w} \mathrm{erf}(\sqrt{x_w}), \quad x_w = \frac{b_w m_p}{\langle m_p \rangle}, \tag{9.3}$$

which reproduces approximately the theoretical relations (4.5) with the correction to the pancake merging discussed in Section 5. For the first and third subsamples the expression

$$N_f = \frac{a_f}{x_f^{1.7}} e^{-x_f} [1 + \mathrm{erf}(\sqrt{x_f})], \quad x_f = \sqrt{\frac{b_f m_f}{\langle m_f \rangle}}, \tag{9.4}$$

reproduces approximately the theoretical relations (4.4) and gives better fits. Here parameters $b_w$and b_f describe the truncated character of fitted PDF whereas parameters a_w and a_f provide its normalization. For velocity of clusters, u, the PDF is found to be well fitted to the expected Gaussian distribution, the expression (9.3) with parameters a_v and b_v fits the velocity dispersion σ_v.

For ΛCDM model these PDFs are plotted in Figs 5 and 6 together with the best fits. It turns out that different PDFs verify the accepted discrimination of two populations of structure elements. For the second subsample the relation

$$\frac{\langle m_p \rangle}{2 l_0} \approx 8(0.5 + 1/\pi)\tau_0^2 \approx 6.55\tau_0^2, \tag{9.5}$$

links the mean wall size $0.5\langle m_p \rangle / l_0$ corrected for the random orientation of walls and sampling cores and the parameter τ_0. For the ΛCDM and OCDM models the parameters τ_u (for all samples) and $\langle m_v/l_0 \rangle$, $\tau_v = \sqrt{\langle m_v/l_0 \rangle / 6.55}$, $\langle 0.5 m_p/l_0 \rangle$ and $\tau_p = \sqrt{\langle m_p/l_0 \rangle / 13.1}$ (for the second subsample) listed in Table 1 are consistent with the simulated amplitude. For the first and third subsamples the distributions plotted in Fig. 6 and corresponding parameter $\langle m_v/l_0 \rangle$ characterize the typical mass of dominant numerous poorer elements and it is about half of that for the second subsample.

The formal precision of these estimates can be taken as ~ 7–10 per cent (precision of fits) but a real precision can be estimated by the comparison with the value of the input parameter τ_0 also listed in Table 1. Differences between results obtained in comoving and redshift spaces do not exceed the reached precision. For the SCDM model the expected and reconstructed parameters differ by a factor of ~ 1.5 what can be partly caused by the strong wall disruption. Moreover, this simple description is correct for $m/l_0 \le 1$ whereas more cumbersome general relations describe the properties of richer walls which dominate the SCDM model.

In all these cases the simulated mass distribution can be equally well fitted to a power law with the exponent $\kappa \sim 1.5$–2. Such distribution is similar to that described analytically for the matter concentration within a set of clusters with a surface density $\sigma_{cls} \propto r^{-\gamma}$ (see also discussion in Miralda-Escude et al. 1996). In this case the measured PDF and mass function are also expressed by the power law

$$dW_{cls} \propto \sigma_{cls} r dr \propto \sigma_{cls}^{-2/\gamma} d\sigma_{cls}. \tag{9.6}$$

Of course, profiles of separate irregular clusters can vary over a wide range and such description and interpretation illustrate only the important role of small-scale clustering.

9.3 Evolution of DM structure

Results obtained in Sections 3, 4 and 5 show that during the most interesting period $\tau \gg l_c/l_0$ evolution of DM structure shows features of self-similarity and important characteristics of structure can be expressed as functions of the parameter $\mu(q)/\tau$. This approximate self-similarity is caused by the Zel'dovich approximation and occurs for any distribution function of initial perturbations and any power spectrum. It becomes more transparent for simple structure functions, at $q_0 \ll q \le 1$ (Appendix A), typical for the CDM like initial power spectrum, but becomes more cumbersome for $\tau \sim l_c/l_0 \ll 1$, and $\tau \ge 1$, when the influence of the scales q_0 and L_0, introduced by (A6), (A7) becomes important. This self-similarity allows us to characterize the structure evolution by the time dependence of several typical parameters such as the mean and median masses, $\langle m \rangle$ and m_m.

This approximate self-similarity is partly violated due to the evolution of pancakes, discussed in Section 4, and small-scale pancake disruption as they are not described by the Zel'dovich theory. Nonetheless, the observations and simulations show that in a universe dominated by cold DM particles general properties of matter distribution are quite similar at high and small redshifts (see more detailed discussion in Governato et al. 1998; Jenkins et al. 1998). Self-similarity of structure evolution was previously discussed for the scale-free power spectra (see, e.g., Efstathiou et al. 1988).

The evolution of observed structure formed by galaxies can however be far from the self-similar evolution of DM structure owing to the small- and large-scale bias. Nonetheless, as it was discussed above, the main parameters of DM structure can be compared with observed galaxy distribution. Thus, in particular, the observed separation of filaments, at $z = 0$, is about 4–6 times smaller then the typical separation of walls (see, e.g., Efstathiou et al. 1988). Such a result can be attributed to pancakes formed by compression of a slice with thickness $m_f \sim (0.1$–$0.05) m_m \approx 1$–$2h^{-1}$ Mpc at redshift $z \sim 3$–5. In smaller pancakes the formation of galaxies can be suppressed and they can be associated with weak Ly-α absorbers observed far from galaxies (Morris et al. 1993; Stocke et al. 1995; Shull, Stocke & Penton 1996).

10 SUMMARY AND DISCUSSION

In this paper we continue investigations and statistical description of the process of structure formation and evolution initiated in our

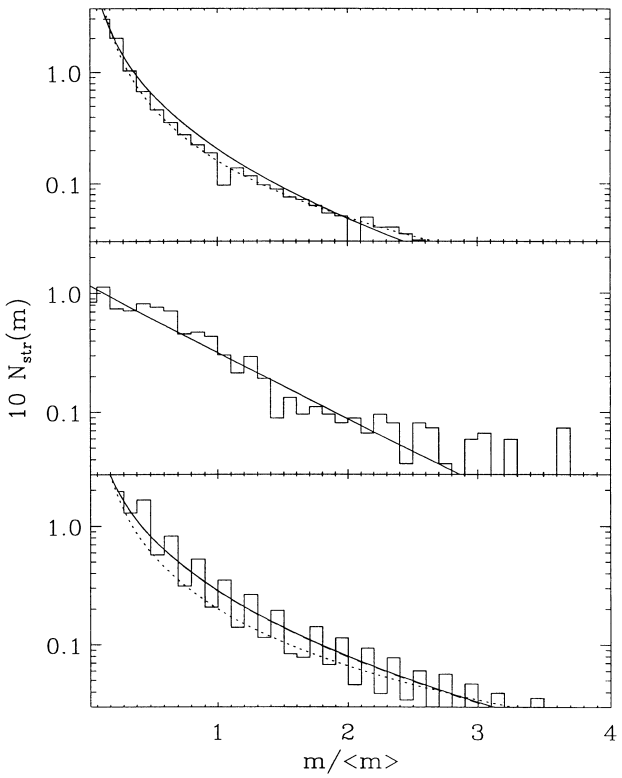

Figure 5. The simulated PDFs of surface density of structure elements, $N_{\rm str}(m)$, versus $m/\langle m\rangle$ for the full sample (top panel) and subsamples of richer (middle panel) and poorer (bottom panel) structure elements for the ΛCDM model. The fits (9.3) and (9.4) are plotted by solid lines, the power fits are plotted by dashed lines.

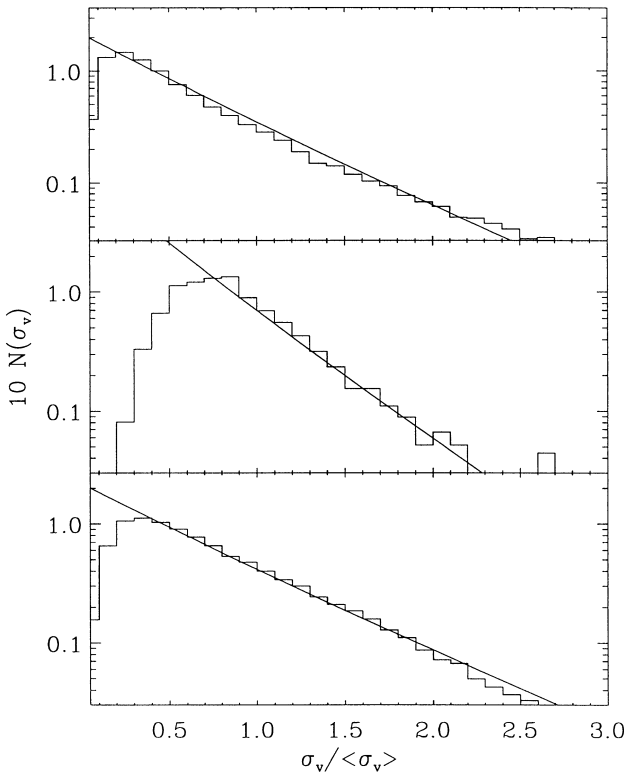

Figure 6. The simulated PDFs of velocity dispersion of structure elements, $N_{\rm str}(\sigma_v)$, versus $\sigma_v/\langle\sigma_v\rangle$ for the full sample (top panel) and subsamples of richer (middle panel) and poorer (bottom panel) structure elements for the ΛCDM model. The fits (9.3) are plotted by solid lines.

previous papers (Buryak, Demiański & Doroshkevich 1992; Demiański & Doroshkevich 1992, 1997; DFGMM; Paper I) and based on the non-linear theory of gravitational instability (Zel'dovich 1970). The new elements discussed above are the approximate statistical description of the non-linear structure evolution manifesting itself as a successive matter concentration into more and more massive structure elements and the estimates of the large-scale modulation of the spatial distribution of luminous matter relative to DM and baryonic components. We show that, as has been discussed in Section 9.4, the evolution of DM structure demonstrates some features of self-similarity and the main characteristics of the DM structure can be expressed through the structure functions of initial perturbations and through parameters of the initial power spectrum and cosmological models. It is shown – in accordance with simulations – that in a low-density models the non-linear evolution occurs on the scale ~ 20–$25h^{-1}$ Mpc and results in formation of wall-like component of the structure of the Universe.

Results discussed in Section 3 show that, for the CDM-like power spectra, the high non-linear matter compression into low-mass pancakes and the percolation take place already at $\tau \approx l_{\rm c}/l_0 \ll 1$. Later evolution leads to a rapid growth of typical mass of DM pancakes. The theoretical description discussed above can be directly applied to the interpretation of deep pencil beam galactic surveys and absorption spectra of quasars, which allows us to consider together rich observational data accumulated by these methods for both small and large redshifts. For larger 3D catalogues and simulations this description can be applied to results obtained with the core-sampling analysis as demonstrated in Section 9.2.

Comparison with simulations shows that the velocity dispersion of matter compressed within the wall-like elements is more sensitive to the cosmological parameters, large-scale modulation of spatial galaxy distribution and properties of DM component. The small-scale clustering generates the essential difference between the expected and simulated velocity dispersion and allows us to discriminate the cosmological models with respect to the matter density, $\Omega_{\rm m}$, and the composition of DM. This clustering is smaller for the models with $\Omega_{\rm m} \leq 0.5$, but for models with $\Omega_{\rm m} \leq 0.3$ it is more difficult to reproduce the sizes, separations of observed walls, and the high matter concentration within the SLSS. The observed structure parameters are best reproduced for the models with $\Omega_{\rm m}h \approx 0.2$–$0.3$. These values are consistent with estimates obtained both from the simulations of cluster of galaxies (Bahcall & Fan 1998; Cole et al. 1997, 1998) and from the observations of high-redshift supernovae (Perlmutter et al. 1998).

Two factors can extend the set of acceptable cosmological parameters. The first is a more complicated composition of DM component, what means that an essential fraction of DM can be associated with relatively hot and/or low-mass particles (see, e.g., Colombi, Dodelson & Widrow 1996; Brustein & Hadad 1999). The simple estimates based on the Trimain–Gunn relation (Trimain & Gunn 1979) show that if the recently formed wall-like SLSS is sensitive to the influence of low-mass relic particles, with $M_{\rm p} \leq 3$–5 eV, then the structure properties at higher redshifts are sensitive to more massive particles as well. This means that for

the MDM models with more complicated DM composition the agreement between observed and simulated properties of the LSS and SLSS can be achieved in a broader range of Ω_m and h and, moreover, the analysis of observed structure evolution can specify the DM composition. The models including some fraction of unstable dark matter particles (Turner, Steigman & Krauss 1984; Doroshkevich, Klypin & Khlopov 1989) seem also to be promising. Unstable particles can produce reheating by photo decay whereas the hot products of decay will delay both formation and disruption of the walls.

The second factor is the large-scale modulation of spatial galaxy distribution. The formation of LSS and SLSS is always accompanied by bias on the same scales, because both processes are caused by the same large-scale perturbations and, so, are strongly correlated in space. The efficiency of such bias depends on many factors, such as the redshift of reheating period, and the formation and evolution of cold clouds. The rough estimates of the bias presented in Section 7 show that the bias factor could be quite high (see also Demiański & Doroshkevich 1997; Paper I) and together with other factors it can essentially distort the spatial distribution of galaxies with respect to the DM distribution. These estimates could be enhanced by taking into account the mutual interaction of pancakes with various sizes and moments of formation. More representative estimates of the bias can, probably, be obtained from simulations such as, for example, Sahni, Sathyaprakash & Shandarin (1994) and Cole et al. (1998).

This mechanism of bias generation implies early, for $z \geqslant 5$, formation of the main fraction of low-entropy gaseous clouds, that can be identified with 'protogalaxies'. The reheating does not prevent further formation of DM pancakes, which can be identified with a population of gas clouds responsible for weaker absorption lines observed at high redshifts (Miralda-Escude et al. 1996; Hernquist et al. 1996) but it inhibits the formation of high-density, low-entropy gaseous clouds and delays the formation of galaxies in extended underdense regions. Further transformation of formed earlier 'protogalaxies' into observed galaxies is a slow and complicated process continuing up to now and earlier formation of such clouds is not in contradiction with the observed peak of galaxy formation at redshifts $z \approx 2$–3 (Steidel et al. 1996).

The observed strong variations of galaxy distribution with respect to the DM and intergalactic gas distribution, ρ_{gal}/ρ_{gas}, can be, partly, associated with this bias. Indeed, if in clusters of galaxies this ratio is found to be $\rho_{gal}/\rho_{gas} \approx 0.2$ (see, e.g., White, Briel & Henry 1993) then, for example, within Boöts Void $\rho_{gal}/\rho_{gas} \to 0$ (Weistrop et al. 1992). The existence of 'invisible' structure elements, which are now seen as gas clouds responsible for weak Ly-α absorption lines situated far from galaxies (≈ 5–$6\,h^{-1}$ Mpc, Morris et al. 1993; Stocke et al. 1995; Shull, Stocke & Penton 1996) can also be considered as an evidence in favour of large-scale bias.

Simulations show also existence of bias in the distribution of DM and 'galaxies' identified with the highest peaks in the initial density distribution (see, e.g., Eke et al. 1996). Such bias is similar, in some important respects, to that generated by reheating. It operates on really large scales (Bower et al. 1993) and can be essential for the SLSS formation as well. It results in structure composed of filaments and sheets in the distribution of 'galaxies' (Doroshkevich et al. 1998a). Other mechanisms of bias formation discussed recently (Coles 1993; Sahni & Coles 1995; Tegmark & Peebles 1998), operate on significantly smaller scales.

Simulations allow us to test the joint action of various factors on the structure parameters and, therefore, they now seem to offer a more prospective way for detailed investigations of the structure formation and evolution. They need, however, to be essentially improved in order to discriminate the spatial distribution and other parameters of 'galaxies' and dark matter. The methods used for the measurement and description of simulated and observed structure should be also improved as now they provide us with limited information about structure properties. These restrictions become especially important at higher redshifts, where the simulated density contrast is small. Large dispersions of measured values make also any comparison of simulated and theoretical structure parameters more difficult. None the less, such an approach seems to be promising because further progress in these directions can be reached.

ACKNOWLEDGMENTS

We are grateful to our referee, Peter Coles, for very useful comments and criticism. This paper was supported in part by Denmark's Grundforskningsfond through its support for an establishment of Theoretical Astrophysics Center and Polish State Committee for Scientific Research grant Nr. 2-P03D-022-10. AGD also wishes to acknowledge support from the Center for Cosmo-Particle Physics 'Cosmion' in the framework of the project 'Cosmoparticle Physics'.

REFERENCES

Babul A., White S. D. M., 1991, MNRAS, 253, 31p
Bahcall N. A., 1988, ARA&A, 26, 631
Bahcall N. A., Fan X., 1998, ApJ, 504, 1
Baltz E. A., Gnedin N. Y., Silk J., 1998, ApJ, 493, L1
Bardeen J. M., Bond J. R., Kaiser N., Szalay A., 1986, ApJ, 304, 15 (BBKS)
Barrow J. D., Bhavsar S. P., Sonoda D., 1985, MNRAS, 216, 17
Bellanger C., de Lapparent V., 1995, ApJ, 455, L103
Bond J. R., Cole S., Efstathiou G., Kaiser N., 1991, ApJ, 379, 440
Bower R. G., Coles P., Frenk C. S., White S. D. M., 1993, ApJ, 405, 403
Broadhurst T. J., Ellis R. S., Koo D. C., Szalay A. S., 1990, Nat, 343, 726
Brustein R., Hadad M., 1999, Phys. Rev. Lett., 82, 3016
Bunn E. F., White M., 1997, ApJ, 480, 6
Buryak O., Demiański M., Doroshkevich A., 1992, ApJ, 393, 464
Buryak O., Doroshkevich A., Fong R., 1994, ApJ, 434, 24
Cohen J. G., Hogg D. W., Pahre M. A., Blandford R., 1996, ApJ, 462, L9
Cole S., Weinberg D. H., Frenk C. S., Ratra B., 1997, MNRAS, 289, 37
Cole S., Hatton S., Weinberg D. H., Frenk C. S., 1998, MNRAS, 300, 945
Coles P., 1993, MNRAS, 262, 1065
Coles P., Davies A. G., Pearson R. C., 1996, MNRAS, 281, 1375
Colombi S., Dodelson S., Widrow L. M., 1996, ApJ, 458, 1
da Costa L. N. et al., 1988, ApJ, 327, 544
de Lapparent V., Geller M. J., Huchra J. P., 1988, ApJ, 332, 44
Dekel A., Silk J., 1986, ApJ, 303, 39
Dekel A., Rees M. J., 1987, Nat, 326, 455
Dekel A., 1997, in da Costa L., ed., Galaxy Scaling Relations: Origin, Evolution and Applications. Springer, Berlin, p. 245
Demiański M., Doroshkevich A., 1992, Int. J. Mod. Phys., D1, 303
Demiański M., Doroshkevich A., 1997, Eighth Marcel Grossman Meeting on General Relativity, in Proc., in press
Demiański M., Doroshkevich A., 1999, ApJ, 512, 527(Paper, I)
Doroshkevich A. G., 1970, Afz, 6, 320
Doroshkevich A., Shandarin S., 1979, SvA, 22, 653
Doroshkevich A. G., 1980, SvA, 24, 152

Doroshkevich A. G., Klypin A. A., Khlopov M. Yu., 1989, MNRAS, 239, 923
Doroshkevich A., Tucker D. L., Oemler A.A., Kirshner R. P., Lin H., Shectman S. A., Landy S. D., Fong R., 1996, MNRAS, 284, 1281 (LCRS1)
Doroshkevich A. G., Fong R., Gottlöber S, Mücket J. P., Müller V., 1997a, MNRAS, 284, 633, (DFGMM)
Doroshkevich A. G., Tucker D. L., Fong R., Turchaninov V., Lin H., 1997b, MNRAS, submitted (LCRS2, preprint TAC 1997-031)
Doroshkevich A., Fong R., Makarova O., 1998a, A&A, 329, 14
Doroshkevich A. G., Fong R., Tucker D., Lin H., 1998b, in Olinto A. V., Frieman J. A., Schramm D. N., eds, Eighteenth Texas Symposium on Relativistic Astrophysics and cosmology: Texas in Chicago. World Scientific, Singapore, p. 560
Doroshkevich A. G., Müller V., Retzlaff J., Turchaninov V. I., 1999a, MNRAS, (DMRT), in press
Doroshkevich A., Fong R., McCracken H. J., Ratcliffe A., Shanks T., Turchaninov V., 1999b, MNRAS, submitted
Dressler A., Faber S. M., Burstein D., Davis R. L., Lynden-Bell D., Terlevich R. J., Wegner G, 1987, ApJ, 313, L37
Efstathiou G., 1992, MNRAS, 256, 43P
Efstathiou G., Frenk C. S., White S. D. M., Davis M., 1988, MNRAS, 235, 715
Einasto M., Einasto J., Tago E., Dalton G., Andernach H., 1994, MNRAS, 269, 301
Eke V. R., Cole S., Frenk C. S., Navarro J. F., 1996, MNRAS, 281, 703
Evrard A. E., Silk J., Szalay A. S., 1990, ApJ, 365, 13
Gorski K. M., Ratra B., Stompor R., Sugiyama N., Banday A. J., 1998, ApJS, 114, 1
Gott J. R. et al., 1989, ApJ, 340, 625
Governato F., Baugh C. M., Frenk C. S., Cole S., Lacey C. G., Quinn T., Stadel J., 1998, Nat, 392, 389
Gregory S. A., Thompson L. A., 1978, ApJ, 222, 784
Hernquist L., Katz N., Weinberg D. H., Miralda-Escude J., 1996, ApJ, 457, L51
Hui L., Kofman L, Shandarin S. F., 1999, preprint (astro-ph/9901104)
Jenkins A. et al., 1998, ApJ, 499, 20
Kendall M., Moran P., 1963, Geometrical Probability. Griffin, London
Kirshner R. P., Oemler A. J., Schechter P. L., Shectman S. A., 1983, AJ, 88, 1285
Kofman L., Bertschinger E., Gelb J. M., Nusser A., Dekel A., 1994, ApJ, 420, 44
Mecke K., Wagner H., 1991, J. Stat. Phys., 64, 843
Melott A. L., Coles P., Feldman H. A., Wilhite B., 1998, ApJ, 496, L85
Miralda-Escude J., Cen R., Ostriker J. P., Rauch M., 1996, ApJ, 471, 582
Morris S. L., Weymann R. J., Dressler A., McCarthy P. J., Smith B. A., Terrile R. J., Giovanelli R., Irwin M., 1993, ApJ, 419, 524
Oort J. H., 1983a, ARA&A., 21, 373
Oort J. H., 1983b, A&A, 139, 211
Peacock J. A., Heavens A. F., 1990, MNRAS, 243, 133
Perlmutter S. et al., 1998, ApJ, in press (astro-ph/9812133)
Quinn T., Katz N., Efstathiou G., 1996, MNRAS, 278, L49
Ramella M., Geller M. J., Huchra J. P., 1992, ApJ, 384, 396
Sahni V., Sathyaprakash B. S., Shandarin S. F., 1994, ApJ, 431, 20
Sahni V., Coles P., 1995, Phys. Rep., 262, 1
Seto N., Yokoyama J., Matsubara T., Siino M., 1997, ApJS, 110, 177
Shandarin S., Zel'dovich Ya. B., 1989, Rev. Mod. Phys., 61, 185
Shapiro P. R., Giroux M. L., Babul A., 1994, ApJ, 427, 25
Shectman S. A., Landy S. D., Oemler A., Tucker D. L., Lin H., Kirshner R. P., Schechter P. L., 1996, ApJ, 470, 172
Shull J. M., Stocke J. T., Penton S. V., 1996, AJ, 111, 72
Steidel C. C., Giavalisco M., Pettini M., Dickinson M., Adlerberg K. L., 1996, ApJ, 462, L17
Stocke J. T., Shull J. M., Penton S. V., Donahue M., Carilli C. 1995, ApJ, 451, 24
Stompor R., Gorski K. M., Bandy A. J., 1995, MNRAS, 277, 1225
Sunyaev R. A., Zel'dovich Ya. B., 1972, A&A, 20, 189
Tegmark M., Silk J., Rees M., Blanchard A., Abel T., Palla F., 1997, ApJ, 474, 1
Tegmark M., Peebles P. J. E., 1998, ApJ, 500, L79
Tomita H., 1990, in Kawasaki K., Suzuki M., Onuki A., eds, Formation, Dynamics and Statistics of Pattern. World Scientific, Singapore
Trimain S., Gunn J. E., 1979, Phys. Rev. Lett., 42, 407
Turner M. S., Steigman G., Krauss L. M., 1984, Phys. Rev. Lett., 52, 2090
Valinia A., Shapiro P. R., Martel H., Vishniac E. T., 1997, ApJ, 479, 46
Vishniac E. T., 1983, ApJ, 274, 152
Weistrop D., Hintzen P., Kennicutt R. C., Liu C., Lowental J., Cheng K. P., Oliversen R., Woodgate B., 1992, ApJ, 396, L23
White S. D. M., Rees M. J., 1978, MNRAS, 183, 341
White S. D. M., Briel U. G., Henry J. P., 1993, MNRAS, 261, L8
Willmer C. N. A., Koo D. C., Szalay A. S., Kurtz M. J., 1994, ApJ, 437, 560
Zel'dovich Ya. B., 1970, A&A, 5, 20
Zel'dovich Ya. B., 1978, in Longair M., Einasto J., eds, Large Scale Structure in the universe. Reidel, Dordrecht, p. 8
Zel'dovich Ya. B., Novikov I. D., 1983, The Structure and Evolution of the Universe. University of Chicago Press, Chicago

APPENDIX A: CORRELATION FUNCTIONS FOR INITIAL PERTURBATIONS

To investigate mutual interaction of perturbations and to reveal their influence on the non-linear processes of structure formation we can use the conventional distribution functions and conventional mean values. In this appendix we introduce a few correlation and structure functions which describe the relative spatial distribution of important parameters of perturbations.

We begin with the structure function of gravitational potential perturbations which characterizes correlation of the gravitational potential in two points $\boldsymbol{q_1}$ and $\boldsymbol{q_2}$. As the power spectrum is a function of the absolute value of wave number $|k|$ only this structure function depends on $q_{12} = |\boldsymbol{q}_1 - \boldsymbol{q}_2|$ and for the perturbations of gravitational potential we have

$$3\frac{\langle \Delta\phi_{12}\Delta\phi_{34}\rangle}{l_0^2\sigma_s^2} = G_0(x_{14}) - G_0(x_{13}) + G_0(x_{23}) - G_0(x_{24}),$$

$$\Delta\phi_{12} = \phi(\boldsymbol{q}_1) - \phi(\boldsymbol{q}_2), \quad \Delta\phi_{34} = \phi(\boldsymbol{q}_3) - \phi(\boldsymbol{q}_4). \tag{A1}$$

Differentiation of this structure function gives other structure functions:

$$\frac{3\langle \Delta\phi(x_{12})S_i(x_3)\rangle}{l_0\sigma_s^2} = (x_1 - x_3)_i G_1(x_{13}) - (x_2 - x_3)_i G_1(x_{23}),$$

$$\frac{3\langle S_i(x_1)S_j(x_2)\rangle}{\sigma_s^2} = \Delta_{ij}G_1(q_{12}) + \frac{x_i x_j}{x^2}G_{12}(x))|_{x=x_{12}},$$

$$\frac{3l_0\langle S_k(x_1)d_{ij}(x_2)\rangle}{\sigma_s^2}$$

$$= (x_k\Delta_{ij} + x_i\Delta_{kj} + x_j\Delta_{ik})G_2(x) + \frac{x_i x_j x_k}{x^2}G_{23}(x))|_{x=x_{21}}, \tag{A2}$$

where the projection operator $\Delta_{ij} = \delta_{ij} - x_i x_j/x^2$ is used and $x = q/l_0$. The scale l_0 was introduced by (2.5).

In the general case these functions can be expressed through the power spectrum, $p(k)$, and spherical Bessel functions and we

obtain

$$G_0(q) = \frac{3}{2\pi^2 l_0^2 \sigma_s^2}\int_0^\infty \frac{p(k)}{k^2}\left(1-\frac{\sin y}{y}\right)\mathrm{d}k, \tag{A3}$$

$$G_1(q) = \frac{3}{(2\pi)^{3/2}\sigma_s^2}\int_0^\infty p(k) y^{-3/2} J_{3/2}(y)\mathrm{d}k = G_0{}'/x,$$

$$G_2(q) = -\frac{3l_0^2}{(2\pi)^{3/2}\sigma_s^2}\int_0^\infty k^2 p(k) y^{-5/2} J_{5/2}(y)\mathrm{d}k = G_1{}'/x,$$

$$G_3(q) = \frac{3l_0^4}{(2\pi)^{3/2}\sigma_s^2}\int_0^\infty k^4 p(k) y^{-7/2} J_{7/2}(y)\mathrm{d}k = G_2{}'/x,$$

where $y = kq$, $x = q/l_0$.

$$G_{12}(x) = G_1(x) + x^2 G_2(x) = G_0'' = (G_1)',$$

$$G_{23}(x) = 3G_2(x) + x^2 G_3(x) = G_{12}'/x, \tag{A4}$$

$$G_{234}(x) = 3G_2(x) + 6x^2 G_3(x) + x^4 G_4(x) = G_{12}''.$$

$$G_1(0) = G_{12}(0) = 1, \quad G_{23}(0) = G_{234}(0) = -\frac{l_0^2}{l_c^2}, \tag{A5}$$

and the scale l_c was introduced by (2.5).

For realistic power spectra these functions cannot be expressed analytically and they have to be calculated numerically. For the Harrison–Zel'dovich primordial power spectrum and for the CDM transfer function (BBKS), for $x = q/l_0 \geq 6l_c^2/l_0^2$, $6l_c^2/l_0^2 \ll 1$ these functions can be approximated by

$$G_0(x) \approx \frac{1}{2a_0}\ln(1 + x + a_0 x^2)$$

$$-\frac{1}{2a_0\sqrt{4a_0-1}}\,tg^{-1}\left(\frac{x\sqrt{4a_0-1}}{2+x}\right),$$

$$G_1(x) \approx [1 + x + a_0 x^2]^{-1}, \tag{A6}$$

$$G_{12}(x) \approx G_1^2(x)[1 - a_0 x^2],$$

$$G_{23}(x) \approx -2G_1^3(x)(1 + 3a_0 x^2 - a_0^2 x^3)/x,$$

$$G_{234}(x) \approx 6G_1^4(x)(1 + 1.3a_0 x^2 + 4a_0^2 x^3 - a_0^3 x^4),$$

$$a_0 = 5(l_0/L_0)^2 \approx 0.3, L_0 \approx 4.1 l_0,$$

where the typical scale L_0 is defined as

$$L_0^2 = 3\pi^2\int_0^\infty p(k)\left(1-\frac{\sin kL_0}{kL_0}\right)k^{-2}\mathrm{d}k \Big/ \int_0^\infty p(k)\mathrm{d}k.$$

The functions (A3) together with fits (A6) are plotted in Fig. A1. The more cumbersome expression

$$G_1(x) \approx (1 + q_0)[1 + \sqrt{q_0^2 + x^2} + a_0 x^2]^{-1}, \tag{A7}$$

$$G_{12} \approx G_1^2(1 + q_0)^{-1}[1 - a_0 x^2 + q_0^2/\sqrt{q_0^2 + x^2}]$$

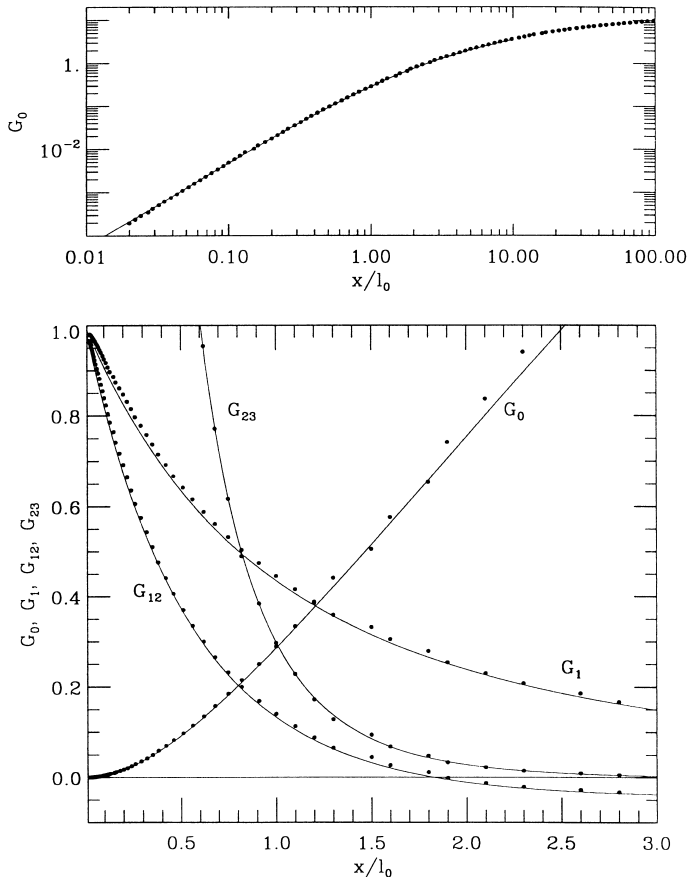

Figure A1. Structure functions G_0 (top panel) and G_0, G_1, G_{12} & $-G_{23}$ versus Lagrangian coordinate q/l_0 for the SCDM power spectrum.

$$q_0 = 6l_c^2/l_0^2[1+\sqrt{1+12l_c^2/l_0^2}]^{-1} \ll 1$$

can be used for all x. In this case the functions $G_2(x)$, $G_{23}(x)$ and $G_{234}(x)$ can be found through the relations (A4).

APPENDIX B: DISTRIBUTION FUNCTION OF PANCAKES

We begin with the distribution function for the difference of displacements at points with coordinates $\boldsymbol{q_1}$ and $\boldsymbol{q_2}$. The normalization and notation introduced in Appendix A are used. The dimensionless 'time' τ is introduced by (2.9).

Let us consider the deformation of spherical cloud with a diameter q. For the case $q \gg q_0$ the general deformation of cloud can be characterized by the 2D random scalar function $\Theta(\theta,\phi) = [\boldsymbol{S}(\boldsymbol{q}/2) - \boldsymbol{S}(-\boldsymbol{q}/2)]\cdot\boldsymbol{q}/q^2$ instead of the deformation tensor d_{ik}. Expansion of this function into spherical harmonics allows one to obtain an approximate description of deformation of the cloud with a reasonable accuracy. Now we will take into account the spherical and quadrupole deformations only. These modes describe successfully the transformation of the cloud into filaments and sheets while higher order deformations relate mainly to the cloud disruption. In this case we can consider the deformation of the cloud in three principal directions, namely, x, y and z. The dispersion of displacement differences in these directions are

$$\sigma_x^2 = \langle[S_x(q/2) - S_x(-q/2)]^2\rangle = 2[1 - G_{12}(q)], \tag{B1}$$

$$\sigma_y^2 = \sigma_z^2 = \sigma_x^2$$

and their correlations are described by the coefficient r_{xy}:

$$\sigma_x^2 r_{xy} = \langle[S_x(q/2) - S_x(-q/2)][S_y(q/2) - S_y(-q/2)]\rangle$$

$$r_{xy} = -\frac{q^2}{2}\frac{G_2(q/\sqrt{2})}{1-G_{12}(q)} \approx \frac{0.25\sqrt{2}}{1+q/2}\left(\frac{1+q}{1+q/\sqrt{2}}\right)^2, \tag{B2}$$

for $q_0 \ll q$. Taking into account the approximate character of our consideration and because of $r_{xy} = r_{xz} = r_{zy} \ll 1$ we will neglect these correlations and will consider the deformation along three principal axes as independent. Under this assumption we have for the distribution of maximal displacement difference $\Delta S_x \geq \Delta S_y \geq \Delta S_z$ and for $\zeta = \Delta S_x/\sigma_x$

$$\frac{dW(\zeta)}{d\zeta} = \frac{3}{4\sqrt{2\pi}}e^{-\zeta^2/2}\left[1+\mathrm{erf}\left(\frac{\zeta}{\sqrt{2}}\right)\right]^2, \zeta \geq 0, \tag{B3}$$

$$\frac{dW(\zeta)}{d\zeta} = \frac{3}{4\sqrt{2\pi}}e^{-\zeta^2/2}\left[1-\mathrm{erf}\left(\frac{\zeta}{\sqrt{2}}\right)\right]^2, \zeta \leq 0.$$

These relations show that under the above assumptions $\sim 1/8$ of matter is compressed in all directions and $\sim 1/8$ expanded in all directions, whereas $\sim 3/8$ of matter is compressed along x and y axes and $\sim 3/8$ of matter is compressed along x axis and expanded along y and z axes. This means that 7/8 of matter is compressed at least along one of the axes. The influence of correlation does not distort the symmetry between compression and expansion and, at $q \leq 1$, increases the probability to find $\Delta S_x \geq \Delta S_y \geq \Delta S_z \geq 0$ up to 0.21.

Let us now consider the matter compression along the direction of maximal compression $\boldsymbol{q} = q_1 - q_2$. In this case the dispersions of displacement differences $\Delta S_i = S_i(q_1) - S_i(q_2)$ are:

$$\sigma_{11}^2 = \langle\Delta S_1 \Delta S_1\rangle = 2[1 - G_{12}(q)],$$

$$\sigma_{22}^2 = \langle\Delta S_2 \Delta S_2\rangle = \sigma_{33}^2 = \langle\Delta S_3 \Delta S_3\rangle = 2[1 - G_1(q)], \tag{B4}$$

$$\langle\Delta S_1 \Delta S_2\rangle = \langle\Delta S_1 \Delta S_3\rangle = \langle\Delta S_2 \Delta S_3\rangle = 0.$$

For the distribution function (B3) the probability to have $\Delta S_1 \geq q/\tau$ is

$$W_{cr}(q) = 1 - \frac{1}{8}\left[1+\mathrm{erf}\left(\frac{\mu(q)}{\sqrt{2}\tau}\right)\right]^3, \tag{B5}$$

$$\mu(q) = \frac{q}{\sqrt{2[1-G_{12}(q)]}}.$$

This function characterizes the intersection of two particles before the time moment τ or for the pancake separation $\geq q$ and, in fact, $(8/7)W_{cr}$ is the cumulative distribution function for pancakes with masses $> q$, for a given τ.

The standard technique (see, e.g., BBKS) can be used in order to find the mean comoving linear density of pancakes with a given $\Delta S_1 = q/\tau$ along a random straight line. It is expressed through the characteristics of the derivations of function Q introduced by (3.2), $Q_i = \partial Q/\partial q_i$, and for $q_0 \ll 1$

$$\langle Q_i\rangle = 0, \quad \sigma_{d1}^2 = \langle Q_1^2\rangle \approx 6/q_0, \tag{B6}$$

$$\sigma_{d2}^2 = \langle Q_2^2\rangle = \sigma_{d3}^2 = \langle Q_3^2\rangle \approx 2/q_0$$

(q_0 is introduced by A7). The required linear number density, $n(>q)$, is

$$l_0 n(>q) = \frac{3\langle\mu_r\rangle}{16\pi^2\sigma_{11}\sigma_{d1}\sigma_{d2}\sigma_{d3}}\Phi\left(\frac{\mu(q)}{\sqrt{2}\tau}\right) \tag{B7}$$

$$\times\int\sqrt{Q_1^2+Q_2^2+Q_3^2}\exp\left[-\frac{Q_1^2}{2\sigma_{d1}^2}-\frac{Q_2^2}{2\sigma_{d2}^2}-\frac{Q_3^2}{2\sigma_{d3}^2}\right]dQ_1 dQ_2 dQ_3$$

where μ_r characterizes the random angle of the intersection. For $l_c/l_0 \ll 1$, and $q \gg q_0$, we obtain (3.10).

APPENDIX C: INTERACTIONS OF PANCAKES

In order to investigate the correlations of the pancake properties we need to consider the intersection of the points q_1 and q_2, $q_{12} = q_1 - q_2$, at the moment τ_1, and points q_3 and q_4, $q_{34} = q_3 - q_4$, at the moments τ_2, respectively. We consider the simplest case when the vectors $\boldsymbol{q}_{12}$ and $\boldsymbol{q}_{34}$ are situated along the same line.

It is convenient to characterize the pancakes by their sizes, D_1 and D_2, and by the separation of their central points, D_{sep}. In this case we have

$$q_{12} = D_1, \quad q_{34} = D_2,$$

$$q_{31} = D_{sep} - 0.5(D_1 - D_2), \quad q_{41} = D_{sep} - 0.5(D_1 + D_2),$$

$$q_{32} = D_{sep} + 0.5(D_1 + D_2), \quad q_{42} = D_{sep} + 0.5(D_1 - D_2).$$

The dispersions and the correlation of displacements $\Delta S(D_1)$ and $\Delta S(D_2)$ can be written as

$$\sigma_1^2(D_1) = \sigma_{11}(D_1), \quad \sigma_2^2(D_2) = \sigma_{11}(D_2), \tag{C1}$$

$$\sigma_1\sigma_2 r_s = G_{12}(q_{31}) - G_{12}(q_{32}) + G_{12}(q_{42}) - G_{12}(q_{41}),$$

and r_s is a symmetric function of D_{sep}. For $D_{sep} \to \infty$ $r_s \to 0$, and for $D_{sep} = 0$

$$\sigma_1\sigma_2 r_s = 2\left[G_{12}\left(\frac{D_1 - D_2}{2}\right) - G_{12}\left(\frac{D_1 + D_2}{2}\right)\right], \tag{C2}$$

$$r_s(D_1, D_2, 0) \approx -\mu(D_1)\mu(D_2)G_{23}(D_1/2), \quad D_2 \ll 1.$$

For $D_{sep} = 0$, $D_1 = D_2$, $r_s = 1$.

For a given $\Delta S(D_1) = D_1/\tau_1$ the conditional mean values $\langle \Delta S_c(D_2, D_{sep})\rangle$ and dispersions $\sigma_c(D_2, D_{sep})$ are described by the standard relations

$$\langle \Delta S_c(D_2, D_{sep})\rangle = \sigma_2 r_s \mu_1/\tau_1, \sigma_c(D_2, D_{sep}) = \sigma_2\sqrt{1 - r_s^2},$$

and the conditional probability of the pancake formation with $\Delta S(D_2, D_{sep}) \geq D_2/\tau_2$ under the condition $\Delta S(D_1) = D_1/\tau_1$ is

$$W_c(> D_2, \tau_2; D_1, \tau_1, D_{sep}) = 0.5\mathrm{erfc}\left(\frac{g_2}{\sqrt{2}}\right). \tag{C3}$$

$$g_2 = \left[\frac{\mu(D_2)}{\tau_2} - r_s\frac{\mu(D_1)}{\tau_1}\right](1 - r_s^2)^{-1/2}.$$

These relations allow us to describe the formation of pancakes with $D_2 \leq D_1$ at the moment $\tau_2 \leq \tau_1$ and, in particular, to find the function $\langle m_{cold}(D_{sep})\rangle$ and $N_m(D_{sep})$. For $\tau_1 = \tau_2$ the same relations describe the accumulation of the smaller pancake (D_2) by the larger one (D_1).

More complicated relations describe the pancake coagulation. As it was noted in Section 3.4 this process is characterized by the function

$$\psi(D_1, D_2, D_{sep}) = \frac{\phi(q_{cent} + D_1/2) - \phi(q_{cent} - D_1/2)}{D_1} - \frac{\phi(D_{sep} + q_{cent} + D_2/2) - \phi(D_{sep} + q_{cent} - D_2/2)}{D_2},$$

and the condition of coagulation is

$$\psi(D_1, D_2, D_{sep}) = D_{sep}/\tau. \tag{C4}$$

To obtain the statistical description of this process the conditional mean value $\langle \psi^c(D_1, D_2, D_{sep})\rangle$ and dispersion σ_ψ^c need to be found. Using the expressions given in Appendix A and notation introduced above we obtain:

$$\frac{1}{2}\sigma_\psi^2 = \frac{G_0(D_1)}{D_1^2} + \frac{G_0(D_2)}{D_2^2} + \frac{G_0(q_{31}) - G_0(q_{41}) - G_0(q_{32}) + G_0(q_{42})}{D_1 D_2}. \tag{C5}$$

The cross-correlation of functions ψ and $\Delta S(q_{12})$, $\Delta S(q_{34})$ is described as following:

$$\frac{\langle \psi\Delta S(D_1)\rangle}{\sigma_\psi\sigma_1} = \mu(D_1)r_\psi, \quad \frac{\langle \psi\Delta S(D_2)\rangle}{\sigma_\psi\sigma_2} = \mu(D_2)r_\psi,$$

$$r_\psi = \frac{q_{31}G_1(q_{31}) - q_{41}G_1(q_{41}) - q_{32}G_1(q_{32}) + q_{42}G_1(q_{42})}{D_1 D_2 \sigma_\psi}.$$

For the conditional mean value and dispersion of ψ we have

$$\frac{\langle \psi^c\rangle}{\sigma_\psi} = r_\psi\left(\frac{[\mu(D_1) - \mu(D_2)]^2}{1 - r_s^2} + \frac{2\mu(D_1)\mu(D_2)}{1 + r_s}\right),$$

$$\left(\frac{\sigma_\psi^c}{\sigma_\psi}\right)^2 = 1 - r_\psi^2\left(\frac{[\mu(D_1) - \mu(D_2)]^2}{1 - r_s^2} + \frac{2\mu(D_1)\mu(D_2)}{1 + r_s}\right).$$

Finally for the required function $\chi(D_1, D_2, D_{sep})$ we obtain

$$\chi = [D_{sep} - \langle \psi^c\rangle]/\sigma_\psi^c. \tag{C6}$$

APPENDIX D: THE DYNAMICAL CHARACTERISTICS OF PANCAKES

A correlation of pancake velocity described by (8.4) in points with different transversal coordinates is conventionally characterized by the correlation coefficient

$$r_v = \frac{\langle[\phi(\boldsymbol{q}_1) - \phi(\boldsymbol{q}_2)][\phi(\boldsymbol{q}_3) - \phi(\boldsymbol{q}_4)]\rangle}{\sqrt{\langle[\phi(\boldsymbol{q}_1) - \phi(\boldsymbol{q}_2)]^2\rangle\langle[\phi(\boldsymbol{q}_3) - \phi(\boldsymbol{q}_4)]^2\rangle}} = \frac{G_0(q_{14}) - G_0(q_{13}) + G_0(q_{23}) - G_0(q_{24})}{2\sqrt{G_0(q_{12})G_0(q_{34})}}. \tag{D1}$$

For small q_{12} and q_{34} it transforms into (8.8).

The important characteristic of the pancake is the velocity profile around the points q_1 and q_2 under the condition $\Delta S(q_{12}) = q_{12}/\tau$. It is described by the mean conditional profile of displacement

$$\langle S(q_3)\rangle = \frac{q_1 - q_2}{\tau}\frac{G_{12}(q_{13}) - G_{12}(q_{23})}{2[1 - G_{12}(q_{12})]}, \tag{D2}$$

and the conditional dispersion

$$\sigma_s^2(q_3) = 1 - \frac{[G_{12}(q_{13}) - G_{12}(q_{23})]^2}{2[1 - G_{12}(q_{12})]}. \tag{D3}$$

Using the expression (8.9) the velocity dispersion within pancakes can be found as follows:

$$\frac{(1+z)^2}{H^2(z)}\sigma_v^2 = \frac{q_{12}^2}{12}[(1 - \beta(z))^2 + 2\beta(z)f_1(q_{12}) - \beta^2(z)f_2(q_{12}) + \tau^2\beta^2(z)f_3(q_{12})], \tag{D4}$$

$$f_1(q_{12}) = 1 - \frac{12}{q_{12}^2}\frac{G_0(q_{12}) - 0.5q_{12}^2G_1(q_{12})}{1 - G_{12}(q_{12})},$$

$$f_2(q_{12}) = 1 - \frac{3J_{12}}{[1 - G_{12}(q_{12})]^2},$$

$$f_3(q_{12}) = 1 - \frac{J_{12}}{2[1 - G_{12}(q_{12})]} - \frac{2G_0(q_{12})}{q_{12}^2},$$

$$J_{12} = q_{12}^{-1}\int_{q_2}^{q_1} dq_3[G_{12}(q_1 - q_3) - G_{12}(q_2 - q_3)]^2.$$

This paper has been typeset from a TEX/LATEX file prepared by the author.